

Semi-Integrated-Sensing-and-Communication (Semi-ISaC): From OMA to NOMA

Chao Zhang, *Graduate Student Member, IEEE*, Wenqiang Yi, *Member, IEEE*,
Yuanwei Liu, *Senior Member, IEEE*, and Lajos Hanzo, *Life Fellow, IEEE*

Abstract

The new concept of semi-integrated-sensing-and-communication (Semi-ISaC) is proposed for next-generation cellular networks. Compared to the state-of-the-art, where the total bandwidth is used for ISaC, the proposed Semi-ISaC framework provides more freedom as it allows that a portion of the bandwidth is exclusively used for either wireless communication or for radar detection, while the rest is for ISaC transmission. To enhance the bandwidth efficiency (BE), we investigate the evolution of Semi-ISaC networks from orthogonal multiple access (OMA) to non-orthogonal multiple access (NOMA). First, we evaluate the performance of an OMA-based Semi-ISaC network. As for the communication signals, we investigate both the outage probability (OP) and the ergodic rate. As for the radar echoes, we characterize the ergodic radar estimation information rate (REIR). Based on these metrics, we derive the analytical and asymptotic expressions of the ergodic RIER. Then, we investigate the performance of a NOMA-based Semi-ISaC network. More specifically, we derive the analytical expressions of both the OP and of the ergodic rate for the communication signals. The asymptotic expressions of OP are also derived for quantifying the diversity gains of the communication signals. As for the radar echoes, we derive the analytical and asymptotic ergodic REIR. The high signal-to-noise ratio (SNR) slopes are also evaluated. The analytical results indicate that: 1) Under a two-user NOMA Semi-ISaC scenario, the diversity order of the near-user equals to the coefficient of the Nakagami- m fading channels (m), while that of the far-user is zero; and 2) The high-SNR slope for the ergodic REIR is based on the ratio of the radar signal's duty cycle and the pulse duration. Our simulation results show that: 1) Semi-ISaC has better channel capacity than conventional ISaC; and 2) NOMA-based Semi-ISaC has better channel capacity than OMA-based Semi-ISaC.

Chao Zhang, Wenqiang Yi, and Yuanwei Liu are the School of Electronic Engineering and Computer Science, Queen Mary University of London, London E1 4NS, U.K. (email:{chao.zhang, w.yi, yuanwei.liu}@qmul.ac.uk).

L. Hanzo is with the School of Electronics and Computer Science, University of Southampton, Southampton, SO17 1BJ, U.K. (e-mail: lh@ecs.soton.ac.uk).

Part of this work has been accepted to IEEE International Conference on Communications (ICC), Seoul, South Korea, May, 2022 [1].

Index Terms

Semi-integrated-sensing-and-communication, non-orthogonal multiple access, orthogonal multiple access, outage probability, ergodic radar estimation information rate

I. INTRODUCTION

Given the incessant escalation of wireless tele-traffic, the impending spectrum-crunch can only be circumvented by the migration to millimeter-wave (mm-wave) carriers. However, since radar sensing technologies also rely on mm-wave carriers, the bandwidth of sensing and wireless communication might become overlapped [2]–[4]. Indeed, it is possible to economize by sophisticated bandwidth-sharing in next-generation wireless communications (6G) with the aid of integrated sensing and communication (ISaC) [5].

In practical scenarios, it is difficult to exploit the total spectrum for ISaC as the bandwidth has already been occupied by a variety of different applications, as exemplified by the L-band (1-2 GHz) for long-range air traffic control and long-range surveillance; the S-band (2-4 GHz) for terminal air traffic control, moderate-range surveillance, and long-range weather observation; the C-band (4-8 GHz) for long-range tracking, weapon location, and weather observation; and the mm-waves for high-resolution mapping, satellite altimetry, vehicular radars, and police radars [6]. Hence, the most practical scenario is that a given portion of the bandwidth is exploited for ISaC in support of its specific applications, while the remaining bandwidth is exploited only for bandwidth-thirsty wireless communications or radar detection. Explicitly, compared to conventional ISaC scenarios, a semi-integrated-sensing-and-communication (Semi-ISaC) solution is more promising for next-generation applications.

For Semi-ISaC, non-orthogonal multiple access (NOMA) appears to be a more promising solution than orthogonal multiple access (OMA), since the successive interference cancellation (SIC) concept fits the ISaC scenarios well. There are several compelling advantages of NOMA-aided Semi-ISaC networks. Firstly, the bandwidth efficiency (BE) is enhanced by NOMA because each resource block is capable of serving multiple users. Additionally, since the SIC scheme is quite mature, we have a strong basis for fundamental analysis to harness the NOMA philosophy in ISaC networks [7], [8]. Moreover, for the conventional ISaC networks, the base station (BS) may need the predicted radar echoes for enhancing the accuracy of computing radar information [9] by enhancing the power difference between communication and radar signals for their detection by SIC. When we exploit the NOMA technique relying on accurate power allocation [7], [10],

the transmit powers of the communication users and that of the BS (for the radar signals) may be accurately controlled for relaxing the accuracy of radar echo prediction. Furthermore, it provides a new degree of freedom for Semi-ISaC networks.

A. Related Works

Based on the advantages of NOMA in Semi-ISaC networks, NOMA-aided Semi-ISaC networks have attracted increasing attention both in academia and in industry. The past decades have witnessed the development of NOMA [7] and more recently of ISaC [8], [11], but there is a paucity of literature on their amalgam.

1) *Related literature of NOMA*: Several decades have passed since the concept of NOMA was first proposed. But in the recent five years, power domain NOMA combined with SIC and power allocation methods has gained popularity [12]–[14]. Realistic imperfect SIC was investigated in [15], while different power allocation algorithms have been proposed in [16]. As a future advance, the optimal power allocation maximizing the achievable sum rate was determined in [17], while user scheduling relying on a low-complexity suboptimal approach was conceived in [18]. Specifically, the authors of [16]–[18] considered NOMA systems using mm-wave carriers which are eminently suitable for ISaC networks. Thus, the investigation of NOMA-based ISaC networks is promising.

2) *Related literature of ISaC*: The fundamental designs of ISaC networks are investigated in [19]–[22], including spectrum sharing methods [19], [20], waveform designs [21], and resource allocation algorithms [22]. The hottest topic in ISaC networks is the investigation of multiple-input-multiple-output (MIMO) ISaC networks, including their MIMO-aided transceiver designs [23]–[27], interference exploitation or interference removal [28]–[30], and the subject of multi-user MIMO ISaC networks [31]. But again, the performance analysis of NOMA-based ISaC is still in its infancy. Since the MIMO and NOMA techniques use different domains for multiple access, their comparison, combination, and cooperation under the concept of MIMO ISaC networks is warranted. Additionally, several authors investigated the average performance of ISaC systems relying on the SIC scheme [9], [32], demonstrating the feasibility of NOMA in Semi-ISaC networks. Hence, there is ample inspiration to pave the way for the evolution of Semi-ISaC networks from OMA to NOMA.

B. Motivation and Contributions

Again, to consider a practical scenario having high BE, we advocate Semi-ISaC networks, where the bandwidth is split into three portions, namely the communication-only bandwidth, the radar-echo-only bandwidth, and the ISaC bandwidth. Since the NOMA and ISaC concepts match each other harmoniously, we commence by investigating OMA-based Semi-ISaC networks first and then evolve it to a NOMA-based scenario. Our main contributions are summarized as follows:

- We propose the novel philosophy of Semi-ISaC networks, where the total bandwidth is split into three portions: the communication-only bandwidth, the radar-echo-only bandwidth, and the ISaC bandwidth. We define both the OMA-based and the NOMA-based Semi-ISaC scenarios. We define three parameters (α_{semi} , β_{semi} , and ϵ_{semi}) for controlling the bandwidth of different scenarios.
- We evaluate the performance of the OMA-based Semi-ISaC network. As for communication signals, we derive the closed-form expressions of the outage probability (OP) and the ergodic rate. As for radar echoes, we characterize the ergodic Radar Estimation Information Rate (REIR).
- We also investigate the performance of NOMA-based Semi-ISaC networks. We consider a pair of user deployment scenarios. For each scenario, we first derive the closed-form expressions of the OP for the communication signals (for both the communication transmitter and the radar target). We then derive the ergodic rate of the communication signals. We also derive the closed-form analytical expressions of the ergodic REIR for the radar echo.
- We evaluate the asymptotic performance of the NOMA-based Semi-ISaC network. Based on the asymptotic expressions, we glean some further insights. We first derive the asymptotic expressions of both the OP and of the ergodic REIR. We then derive both the diversity order of communication signals and the high-SNR slopes for characterizing the radar echoes. As for the diversity orders, analytical results indicate that the near-user's diversity order is m , which is the parameter of Nakagami- m fading channels, while the far-user's diversity gain is zero. As for the high-SNR slopes of the ergodic REIR, we observe that the high-SNR slope is related both to the radar's duty cycle and to the pulse duration during its transmission from the BS to the radar target. We also extend the derivations by varying the coefficients (α_{semi} , β_{semi} , and ϵ_{semi}) for controlling the resource allocation of the Semi-ISaC system.

- Our numerical results illustrate the following conclusions. 1) For the communication signals, increasing the line-of-sight (LoS) component's power enhances the outage performance. 2) For the radar echo, dense pulses emerging from the BS enhance the performance of radars. 3) The high-SNR slopes of the radar echo are also related to the radar's duty cycle and pulse duration, separately.

C. Organizations

The paper is organized as follows. In Section II, we introduce the OMA/NOMA-based Semi-ISaC concepts. In Section III, we investigate the performance of OMA-based Semi-ISaC networks. In Section IV, we evaluate the analytical performance of NOMA-aided Semi-ISaC networks, including the analytical outage performance, the ergodic rates of communication signals, as well as the ergodic REIR of the radar echoes. In Section V, we evaluate the system's asymptotic performance and provide insights concerning the NOMA-assisted Semi-ISaC networks, including their asymptotic outage performance for the communication signals having diversity gains and the asymptotic ergodic REIR of the radar echoes by relying on the high-SNR slopes. We then present our numerical results in Section VI, followed by our conclusions in Section VII.

II. SYSTEM MODEL

We focus our attention on an the uplink (UL) of Semi-ISaC systems, which includes a BS, a communication transmitter, and a radar target. A single-input-single-output (SISO) model is considered. We assume that the radar target also has communication functions, as exemplified by cars or unmanned aerial vehicles. To design the Semi-ISaC system, the total bandwidth B is split into three portions, including the bandwidth for wireless communication (denoted as B_W), the bandwidth for ISaC (denoted as B_I), and the bandwidth for radar detection (denoted as B_R). We define three coefficients (α_{semi} , β_{semi} , and ϵ_{semi}) for controlling the bandwidth of different scenarios as:

$$B = \underbrace{\alpha_{semi}B}_{B_R} + \underbrace{\beta_{semi}B}_{B_I} + \underbrace{\epsilon_{semi}B}_{B_W}. \quad (1)$$

where $\alpha_{semi} \in [0, 1]$, $\beta_{semi} \in [0, 1]$, $\epsilon_{semi} \in [0, 1]$, and $\alpha_{semi} + \beta_{semi} + \epsilon_{semi} = 1$.

Before introducing the Semi-ISaC channel model, we highlight our assumptions as follows:

- 1) There is only one radar target located in the serving area of the ISaC BS. Other radar targets are served by the BSs of other cells, and hence are ignored in our analysis.

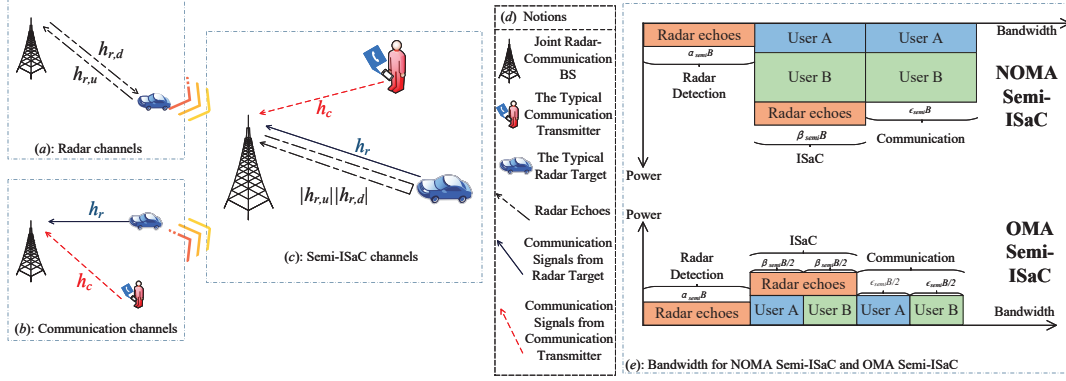


Fig. 1. Illustration of the NOMA-based Semi-ISaC system: (a) Channels in conventional radar detection systems; (b) Channels in conventional UL NOMA systems; (c) Channels in NOMA-based Semi-ISaC systems; (d) Notations; and (e) The bandwidth utilization for the NOMA-based Semi-ISaC systems and OMA-based Semi-ISaC systems;

- 2) Based on prior observations, the BS is capable of accurately predicting and estimating the time delay of radar echoes to avoid synchronization errors.
- 3) The range resolution of the radar system is sufficiently accurate for avoiding the interference between two radar targets.
- 4) The range fluctuation is interpreted as a time-delay fluctuation modeled by the Gaussian distribution [9].
- 5) The cross-section of the radar target considered is represented by a constant parameter, denoted as σ_{RCS} . The Doppler shift estimation is perfect for the radar targets in order to predict and correct the waveforms.

A. Frequency-division (FD) ISaC, OMA-based Semi-ISaC and NOMA-based Semi-ISaC

This subsection presents the fundamental concepts and definitions of the conventional (FD) ISaC, OMA-based Semi-ISaC, and NOMA-based Semi-ISaC.

1) *FD ISaC*: Our benchmark is the FD ISaC having the coefficients of $\alpha_{semi}=0$, $\beta_{semi}=1$, and $\epsilon_{semi}=0$. The total bandwidth B is exploited for the ISaC scenario. The users are assigned to orthogonal resource blocks. The BE is hence reduced.

2) *OMA-based Semi-ISaC*: The total bandwidth B is split into three portions with the constraints in Eq. (1) as $\alpha_{semi} \in [0, 1]$, $\beta_{semi} \in (0, 1]$, $\epsilon_{semi} \in [0, 1]$, and $\alpha_{semi} + \beta_{semi} + \epsilon_{semi} = 1$ (which means $\beta_{semi} \neq 0$). In the ISaC bandwidth, SIC is utilized for extracting the radar echo and communication signals from the superimposed signals, while SIC is not utilized in the rest of the bandwidth. In the following, we consider a two-user case, namely the user A and B. As the radar-echo-only bandwidth (B_R) has no communication signal, OMA is used both

in the ISaC bandwidth (B_I) and in the communication-only bandwidth (B_W). Hence, B_I and B_W are further divided into two OMA sub-bands for the two users, respectively. As shown in Fig. 1. (e), the total bandwidth is finally divided into five parts, including the radar-echo-only bandwidth B_R , the ISaC bandwidth for user A ($B_I/2$), the ISaC bandwidth for user B ($B_I/2$), the communication-only bandwidth for user A ($B_W/2$), and the communication-only bandwidth for user B ($B_W/2$).

3) *NOMA-based Semi-ISaC*: As indicated at the top of Fig. 1. (e), the total bandwidth is split into three portions (B_W , B_I , and B_R) subject to the same coefficient constraints as the OMA-based semi-ISaC. However, wireless communication in the bandwidth B_W and B_I relies on NOMA instead of OMA. As exemplified by a two-user case, the users share the same bandwidth instead of being split into two OMA sub-bands. Additionally, the NOMA-based Semi-ISaC system has to activate SIC in the ISaC bandwidth twice to obtain the radar detection information, while the OMA-based Semi-ISaC scenario only once.

Since the specific locations of the pair of users directly influence the SIC-based detection orders, we consider two specific deployment scenarios: i) A near communication transmitter is paired with a far radar target, termed as *Scenario-I*; and ii) A far communication transmitter is paired with a near radar target, referred to as *Scenario-II*. In the following sections, we evaluate the system performance based on these two scenarios.

B. Channel Model

1) *Small-Scale Fading*: The path loss model and small-scale fading model are defined in this subsection for both the radar and communication links. As the ISaC channels are hosted in the mm-wave band, we assume that Nakagami- m fading is encountered both by the radar and communication channels [32]. The probability density function (PDF) can be expressed as $f_{|h_i|^2}(x) = \frac{m^m}{\Gamma(m)} x^{m-1} \exp(-mx)$, with m being the Nakagami- m shape parameter and its mean value is one. As seen in Fig. 1. (a)-(c), the subscripts $i = \{(r, d), (r, u), r, c\}$ represent different small-scale channel gains, where $|h_{r,d}|^2$ and $|h_{r,u}|^2$ are those of the downlink (DL) transmission and the UL echo of the radar target, $|h_c|^2$ is that of the communication transmitter's UL signal, and $|h_r|^2$ is that of the radar target's UL communication signal.

2) *Large-Scale Fading*: The path loss models of radar echoes are different from communication signals. Assume that the distance between the BS and the communication transmitter is

d_c and the distance between the BS and the radar target is d_r . For the communication channels, the path loss follows the conventional model of

$$\mathcal{P}_c(d_c) = C_c(d_c)^{-\alpha_c}, \quad (2)$$

where α_c is the path loss exponent of communication links, $C_c = \left(\frac{c}{4\pi f_c}\right)^2$ is associated with the reference distance of $d_0 = 1$ m, the speed of light is $c = 3 \times 10^8$ m/s, and the carrier frequency is f_c .

We use different coefficients but present the path loss function of the radar echoes in the same form as in Eq. (2):

$$\mathcal{P}_r(d_r) = C_r(d_r)^{-\alpha_r}, \quad (3)$$

where α_r is the path loss exponent of the radar echoes with $\alpha_r = 4$ representing the free-space scenario [32]. The parameter $C_r = \frac{\sigma_{RCS}\lambda^2}{(4\pi)^3}$ is the reference-distance-based intercept, λ is the wavelength of the carrier, and $\sigma_{RCS} = \frac{4\pi S_r}{S_t}$ is associated with the target radar cross section, where S_r is the power density that is intercepted by the target and S_t is the scattered power density at the reference distance of $d_0 = 1$ m [32].

C. SIC-based Detection Orders for NOMA

The SIC processes of conventional NOMA systems and NOMA-based Semi-ISaC systems are different. For the conventional NOMA systems, the BS only receives signals at two different power levels, when a two-user case is considered, where the near-users receive higher power and are detected first¹. For Semi-ISaC NOMA-based systems under a two-user case, the BS receives a superposition of signal components, i.e. the communication signal from the radar target, the communication signal from the communication transmitter, and the radar echo reflected by the radar target. As the BS is capable of estimating the radar echo, we can subtract the estimated radar echo from the superimposed signals to reduce its interference inflicted upon other communication signals. Hence, the communication signals detected from the two paired users have higher power levels and thus higher priority than the radar echo. As a consequence, it is better to fix the SIC-based detection order of the radar echo to be the last. For the two communication signals, the near-user's signal is detected first and the far-user's signal is detected at the middle stage [9].

¹As fixed power allocation, the path loss has more dominant effects than the small-scale fading, as we consider the average performance. Thus, we consider the near-user to be the strong user [33]

D. Signal Model

We assume that the BS has acquired prior observations to evaluate the predicted range of the radar target positions. Naturally, the uncertainty in the positioning directly corresponds to time delay fluctuations in radar systems [9]. As stated in the assumptions, the time delay fluctuation τ obeys a Gaussian distribution with the variance of $\sigma_\tau^2 = \mathbb{E}[|\tau - \tau_{pre}|^2]$, where $\mathbb{E}[\cdot]$ is the expectation. Based on [9], we derive the average power level of the radar echo by considering the uncertainty in the positioning decision as:

$$\mathbb{E}[|x(t - \tau) - x(t - \tau_{pre})|^2] \approx \gamma^2 \beta_{semi}^2 B^2 \sigma_\tau^2, \quad (4)$$

where we have $\gamma^2 = (2\pi)^2/12$ for a flat spectral shape. The variance τ is the observation of the time delay for the radar target and τ_{pre} is the predicted value of τ .

As we fix the SIC-based detection order of the radar echo to be the last, a drawback has to be tolerated, namely that when the radar echo has a high received power level, the ISaC system may face eroded performance, since the radar echo is regarded as interference for the communication signals in the SIC step. To mitigate this, we exploit the predicted target range to generate a predicted radar return and subtract it from the superimposed signals [9]. We assume that the predicted radar echo is accurate enough for the SIC process. By harnessing this approach, the performance of the communication system is improved. Hence, the received superimposed aggregate signal $v(t)$ is expressed as:

$$\begin{aligned} v(t) = & \underbrace{h_c \sqrt{P_c \mathcal{P}_c(d_c)} z(t)}_{s_c} + \underbrace{h_r \sqrt{P_r \mathcal{P}_r(d_r)} y(t)}_{s_r} \\ & + \underbrace{h_{r,d} h_{r,u} \sqrt{P_{BS} \mathcal{P}_r(d_r)} [x(t - \tau) - x(t - \tau_{pre})]}_{e_r} + n(t), \end{aligned} \quad (5)$$

where s_c is the communication signal received from the UL communication transmitter at the BS, s_r represents the communication signal received from the radar target at the BS, and e_r is the radar echo reflected from the radar target impinging at the BS. Additionally, P_c and P_r are the UL transmit power of the communication transmitter and the radar target, respectively. Moreover, P_{BS} is the UL transmit power of the BS used for radar detection. Finally, $n(t)$ represents the noise having a variance of $\sigma^2 = k_B T_{temp} B$, where k_B is the Boltzmann constant and T_{temp} is the absolute temperature.

Based on the assumptions and derivations above, the signal models of the OMA-based Semi-

ISaC and NOMA-based Semi-ISaC are presented in the following part.

1) *Communication Signals for OMA-based Semi-ISaC*: The signal-to-interference-and-noise ratio (SINR) expression of the communication transmitter and the radar target is expressed as:

$$\gamma_j^{OMA} = \frac{P_j \mathcal{P}_c(d_j) |h_j|^2}{P_{BS} \mathcal{P}_r(d_r) |h_{r,d}|^2 |h_{r,u}|^2 \gamma^2 \beta_{semi}^2 B^2 \sigma_\tau^2 + \sigma^2}, \quad (6)$$

where $j \in \{c, r\}$ represents for the communication transmitter and the radar target, respectively.

2) *Communication Signals for NOMA-based Semi-ISaC in Scenario-I*: For Scenario-I, the communication transmitter is the near-user, whose signals are detected first. Given the different power levels, the BS directly detects the UL signal received from the communication transmitter by considering both the communication signals and the radar echoes of the radar target as interference. Hence, the SINR of the communication transmitter is

$$\gamma_c^I = \frac{\overbrace{P_c \mathcal{P}_c(d_c) |h_c|^2}^{\text{Transmitter's Communication Signals}}}{\underbrace{P_r \mathcal{P}_c(d_r) |h_r|^2}_{\text{Radar's Communication Signals}} + \underbrace{P_{BS} \mathcal{P}_r(d_r) |h_{r,d}|^2 |h_{r,u}|^2 \gamma^2 \beta_{semi}^2 B^2 \sigma_\tau^2}_{\text{Radar Echoes}} + \underbrace{\sigma^2}_{\text{Noise}}}. \quad (7)$$

After detecting, remodulating, and finally subtracting the signal of the communication transmitter from the composite signal by the SIC process, the SINR of the communication signals for the radar target becomes

$$\gamma_r^I = \frac{P_r \mathcal{P}_c(d_r) |h_r|^2}{P_{BS} \mathcal{P}_r(d_r) |h_{r,d}|^2 |h_{r,u}|^2 \gamma^2 \beta_{semi}^2 B^2 \sigma_\tau^2 + \sigma^2}. \quad (8)$$

3) *Communication Signals for NOMA-based Semi-ISaC in Scenario-II*: For Scenario-II, the near-user is the radar target, thus the SIC-based detection orders of the two users (the radar target and the communication transmitter) are swapped. The BS firstly detects the communication signals of the radar target, yielding an SINR of

$$\gamma_r^{II} = \frac{\overbrace{P_r \mathcal{P}_c(d_r) |h_r|^2}^{\text{Radar's Communication Signals}}}{\underbrace{P_c \mathcal{P}_c(d_c) |h_c|^2}_{\text{Transmitter's Communication Signals}} + \underbrace{P_{BS} \mathcal{P}_r(d_r) |h_{r,d}|^2 |h_{r,u}|^2 \gamma^2 \beta_{semi}^2 B^2 \sigma_\tau^2}_{\text{Radar Echoes}} + \underbrace{\sigma^2}_{\text{Noise}}}. \quad (9)$$

Following the SIC process, the SINR of communication signals for the communication trans-

mitter becomes

$$\gamma_c^{II} = \frac{P_c \mathcal{P}_c(d_c) |h_c|^2}{P_{BS} \mathcal{P}_r(d_r) |h_{r,d}|^2 |h_{r,u}|^2 \gamma^2 \beta_{semi}^2 B^2 \sigma_\tau^2 + \sigma^2}. \quad (10)$$

4) *Radar Echoes for OMA and NOMA*: Since we aim to ensure the priority of communication signals, the radar echo is simply left behind after the last SIC stage. Hence, when relying on SIC to detect and remove all communication signals, the SNR is expressed as:

$$\gamma_r^{echo} = \frac{P_{BS} \mathcal{P}_r(d_r) |h_{r,d}|^2 |h_{r,u}|^2 \gamma^2 \beta_{semi}^2 B^2 \sigma_\tau^2}{\sigma^2}. \quad (11)$$

In Section III to V, we will consider the ergodic REIR metric for characterizing the performance of the radar system. This metric is directly related to γ_r^{echo} derived above.

III. PERFORMANCE EVALUATION FOR OMA-BASED SEMI-ISAC

In this section, we evaluate the OMA-based Semi-ISaC networks. Again, we adopt the OP and the ergodic rate as the performance metrics for communication signals. Likewise, the ergodic REIR is adopted as the performance metric for the radar echoes.

A. Performance Evaluation for Communication Signals

In this subsection, we aim to investigate the performance of communication signals. Before that, we first evaluate the average interference strength.

Lemma 1. To simplify the expression of interference (radar echoes), we introduce the shorthand of $I_R = P_{BS} \mathcal{P}_r(d_r) \times |h_{r,d}|^2 |h_{r,u}|^2 \gamma^2 B^2 \sigma_\tau^2$. The expectation of interference is expressed as:

$$\mathbb{E}[I_R](d_r) = P_{BS} \mathcal{P}_r(d_r) \gamma^2 \beta_{semi}^2 B^2 \sigma_\tau^2. \quad (12)$$

Sketch of Proof: Given the definition of expectation and the distribution of Nakagami-m fading channels, the expression of interference is presented as:

$$\mathbb{E}[I_R](d_r) = P_{BS} \mathcal{P}_r(d_r) \gamma^2 \beta_{semi}^2 B^2 \sigma_\tau^2 \left(\frac{m^m}{\Gamma(m)} \right)^2 \int_0^\infty x^m \exp(-mx) dx \int_0^\infty y^m \exp(-my) dy, \quad (13)$$

and with the aid of Eq. [2.3.3.1] in [34], this lemma is proved. We have the detailed proof in Section I of [35].

In OMA-based Semi-ISaC networks, the OP of the communication signals is defined as $\mathbb{P}_j^{OMA} = \Pr \{ \gamma_j^{OMA} < \gamma_{th}^{OMA} \}$, given the threshold γ_{th}^{OMA} . The achieved rate is defined as $R_j^{OMA} = \frac{1}{2} \log_2 (1 + \gamma_j^{OMA})$. **Theorem 1** provides the closed-form expressions of both the OP and of the ergodic rate for communication signals in the OMA-based Semi-ISaC network.

Theorem 1. Upon introducing the subscript of $j \in \{c, r\}$ for representing the communication transmitter and the radar target, the expressions of the OP and of the ergodic rate are derived respectively as:

$$\mathbb{P}_j^{OMA} = \frac{\gamma(m, \Omega \gamma_{th}^{OMA})}{\Gamma(m)}, \quad (14)$$

$$R_j^{OMA} = \frac{1}{2 \ln 2} \sum_{k=0}^{m-1} \exp(\Omega) E_{1+k}(\Omega), \quad (15)$$

where we have $\Omega = \frac{m(P_{BS} \mathcal{P}_r(d_r) \gamma^2 \beta_{semi}^2 B^2 \sigma_\tau^2 + \sigma^2)}{P_j \mathcal{P}_c(d_j)}$, $\Gamma(x)$ is the Gamma function, $\gamma(a, b)$ is the incomplete Gamma function, and $E_n(\cdot)$ is the generalized exponential.

Sketch of Proof: We derive the OP by exploiting the CDF of the Gamma distribution $F_{|h_j|^2}(x) = \frac{\gamma(m, mx)}{\Gamma(m)}$. We additionally derive the ergodic rate by exploiting $\gamma(m, t) = (m-1)! - \exp(-t) \sum_{k=0}^{m-1} \frac{(m-1)!}{k!} t^k$, $\Gamma(-k, \Omega) = \frac{E_{1+k}(\Omega)}{\Omega^k}$ and $\int_0^\infty \frac{x^a}{1+x} \exp(-bx) = \exp(b) \Gamma(a+1) \Gamma(-a, b)$, where $\Gamma(a, b)$ is the incomplete Gamma function. The detailed proof is presented in Section II of [35].

B. Performance Evaluation for Radar Echoes

Again for radar echoes, prior work in [9] has proposed the REIR metric to evaluate the performance of radar targets. This REIR metric may also be further characterized by the Cramér-Rao lower bound [36], [37], which represents a clear relationship between the REIR and the SNR γ_r^{echo} , presented as:

$$R_{est} \leq \frac{\delta}{2T} \log_2 (1 + 2T \beta_{semi} B \gamma_r^{echo}), \quad (16)$$

where $\gamma_r^{echo} = \frac{P_{BS} \mathcal{P}_r(d_r) |h_{r,d}|^2 |h_{r,u}|^2 \gamma^2 \beta_{semi}^2 B^2 \sigma_\tau^2}{\sigma^2}$ is the SNR for the radar echoes of the radar target, T is the radar pulse duration, and δ is the radar's duty cycle of radar targets. We then use the ergodic REIR for quantifying the average radar estimation rate, which may be viewed as the

dual counterpart of the data information rate, presented as:

$$R_{est} \leq \mathbb{E} \left[\frac{\delta}{2T} \log_2 (1 + 2T\beta_{semi}B\gamma_r^{echo}) \right]. \quad (17)$$

1) *Equivalent Radar Channels*: The radar channel may be considered as a pair of independent serially concatenated links, constituted by the DL spanning from the BS to the radar target and the UL link reflected from the radar target back to the BS. Thus, the equivalent small-scale channel gain may be expressed by $|h_{r,eq}|^2 = |h_{r,d}|^2|h_{r,u}|^2$. We first derive the distribution of $|h_{r,eq}|^2$ in **Lemma 2**, based on which the ergodic REIR is given in **Theorem 2**.

Lemma 2. If both links are Nakagami- m fading channels, the PDF and cumulative distribution function (CDF) of the equivalent channel gain is expressed as:

$$f_{|h_{r,eq}|^2}(z) = \frac{2m^{2m}}{(\Gamma(m))^2} z^{m-1} K_0(2m\sqrt{z}), F_{|h_{r,eq}|^2}(z) = \frac{G_{13}^{21}(m^2x|_{m,m,0}^1)}{(\Gamma(m))^2}, \quad (18)$$

where $K_0(\cdot)$ is the modified Bessel function of the third kind and $G_{p\ q}^{mn}(\cdot|_{(b_q)}^{(a_p)})$ is the Meijer G function.

Sketch of Proof: We derive the above PDF and CDF by noticing $K_v(x) = \frac{1}{2}G_{02}^{20}\left(\frac{x^2}{4}\middle|\frac{\cdot}{\frac{v}{2}},\frac{\cdot}{\frac{v}{2}}\right)$, $z^p G_{p\ q}^{mn}\left(z\middle|\frac{(a_p)}{(b_q)}\right) = G_{p\ q}^{mn}\left(z\middle|\frac{(a_p)+p}{(b_q)+p}\right)$, $\int_0^x z^{m-1} G_{02}^{20}(m^2z|_{00}^2) dz = x^m G_{13}^{21}(m^2y|_{0,0}^{1-m,\cdot,-m})$, and Eq.[2.3.6.7] in [34]. We present the comprehensive proof in Section III of [35].

2) *Ergodic REIR*: Based on the equivalent channel distribution, we will derive the ergodic REIR of the radar echoes in **Theorem 2**. We will also exploit **Corollary 1** to evaluate the performance under the Rayleigh fading channels.

Theorem 2. For the analytical results of the radar echoes, the expressions of the ergodic REIR are formulated as:

$$R_{est}^{low} = \frac{\delta}{2T \ln(2)} \int_0^\infty \frac{1}{z+1} \left(1 - \frac{G_{13}^{21}\left(\frac{m^2 d_t^{\alpha_r}}{\Xi_{r,1}} z \middle|_{m,m,0}^1\right)}{(\Gamma(m))^2} \right) dz, \quad (19)$$

where we have $\Xi_{r,1} = 2T\beta_{semi}B\gamma_r^{echo}$.

Sketch of Proof: With the aid of **Lemma 2**, this theorem is proved. The comprehensive proof is presented in Section IV of [35].

Corollary 1. Assuming that the radar channel experiences Rayleigh fading, the ergodic rate in

Eq. (19) is simplified as:

$$R_{est}^{low} = \frac{\delta}{2T \ln(2)} G_{13}^{31} \left(d_t^{\alpha_r} \Xi_{r,1}^{-1} \middle| \begin{smallmatrix} 0 \\ 0,0,1 \end{smallmatrix} \right). \quad (20)$$

*Sketch of Proof: This corollary is proved by exploiting Eq.[2.3.4.4] in [34] and the Meijer G function. Detailed derivations are similar to those of **Lemma 2**. The comprehensive proof is jointly presented in Section IV of [35] with the **Theorem 2**.*

IV. ANALYTICAL PERFORMANCE EVALUATION FOR NOMA-BASED SEMI-ISAC

In this section, we analyze the performance metrics for NOMA-based Semi-ISaC networks. The analytical results in this section will be useful in Section V to obtain deep insights.

A. Performance Analysis for Communication Signals in Scenario-I

Recall that the communication transmitter is the near-user and the radar target is the far-user in Scenario-I. The OP expressions for the NOMA users in Scenario-I are given by

$$\mathbb{P}_c^I = \Pr \{ \gamma_c^I < \gamma_{th} \}, \quad (21)$$

$$\mathbb{P}_r^I = 1 - \Pr \{ \gamma_c^I > \gamma_{SIC}, \gamma_r^I > \gamma_{th} \}, \quad (22)$$

where $\Pr \{A, B\}$ is the probability that both A and B are true, γ_{SIC} is the threshold of the SIC process, and γ_{th} is the threshold of communication signal transmission in the NOMA-based Semi-ISaC scenario. We note that the definition of the threshold is calculated based on the target rate R_{th} , which is $\gamma_{th} = 2^{R_{th}} - 1$. If the OP is lower than the threshold, the communication fails and vice versa.

In the following, the closed-form expressions of the OP and the ergodic rate for a pair of NOMA users are given in **Theorem 3-4** and **Corollary 2-3**.

Theorem 3. In Scenario-I of the NOMA-based Semi-ISaC scenario, the OP expression of the communication transmitter is

$$\begin{aligned} \mathbb{P}_c^I = & 1 - \exp \left(-\frac{m\gamma_{th}}{P_c} (a_1 + a_2) \right) \sum_{p=0}^{m-1} \frac{m^r \gamma_{th}^p}{(m-1)!p!} \\ & \times \sum_{r=0}^p C_p^r \frac{(a_1 + a_2)^r (P_r a_3)^{p-r}}{P_c^p} \Gamma(m+p-r) \left(\frac{\gamma_{th} a_3 P_r}{P_c} + 1 \right)^{-(m+p-r)}, \end{aligned} \quad (23)$$

where we have $a_1 = \frac{P_{BS} G_r C_r (d_r)^{-\alpha_r} \gamma^2 \beta_{semi}^2 B^2 \sigma_r^2}{G_c C_c (d_c)^{-\alpha_c}}$, $a_2 = \frac{\sigma^2}{G_c C_c (d_c)^{-\alpha_c}}$, $a_3 = \frac{(d_r)^{-\alpha_c}}{(d_c)^{-\alpha_c}}$, and $C_n^m = n! / (m! (n-m)!)$.

Sketch of Proof: See Appendix A.

Corollary 2. In Scenario-I, the ergodic rate of the communication transmitter in the NOMA-based Semi-ISAC scenario is formulated as:

$$R_c^{er,I} = \frac{1}{\ln 2} \sum_{p=0}^{m-1} \sum_{r=0}^p C_p^r \frac{\Lambda_1^{r-(1+p+k)} (P_r a_3)^{p-r}}{(m-1)! p! P_c^{p-r}} \Gamma(m+p-r) \sum_{k=0}^{\infty} \binom{m+p-r+k-1}{k} \times \left(-\frac{a_3 P_r}{P_c} \right)^k \exp(\Lambda_1) \Gamma(p+k+1) E_{1+p+k}(\Lambda_1), \quad (24)$$

where we have $\Lambda_1 = \frac{m(a_1+a_2)}{P_c}$.

Sketch of Proof: By substituting the equation in Theorem 3 into the definition of the ergodic rate, which is expressed as $R_c^{er,I} = \frac{1}{\ln 2} \int_0^{\infty} \frac{1 - \mathbb{P}_c^I(\gamma_{th})}{1 + \gamma_{th}} d\gamma_{th}$, the ergodic expression is given by

$$R_c^{er,I} = \frac{1}{\ln 2} \sum_{p=0}^{m-1} \frac{m^r}{(m-1)! p!} \sum_{r=0}^p C_p^r \frac{(a_1 + a_2)^r (P_r a_3)^{p-r}}{P_c^p} \times \Gamma(m+p-r) \int_0^{\infty} \frac{x^p}{1+x} \left(\frac{x a_3 P_r}{P_c} + 1 \right)^{-(m+p-r)} \exp \left(-\frac{m x}{P_c} (a_1 + a_2) \right) dx. \quad (25)$$

The corollary can be proved by noting $(1+x)^{-n} = \sum_{k=0}^{\infty} \binom{n+k-1}{k} (-x)^k$, $\Gamma(a, b) = \sum_{p=0}^{a-1} \frac{(a-1)!}{p!} b^p \times \exp(-b)$, $E_n(x) = x^n \Gamma(1-n, x)$, and $\int_0^{\infty} \frac{x^a}{1+x} \exp(-bx) = \exp(b) \Gamma(a+1) \Gamma(-a, b)$. We have the detailed proof in Section V of [35].

Theorem 4. In Scenario-I of NOMA-based Semi-ISaC, the OP of the radar target is given by

$$\mathbb{P}_r^I = 1 - \sum_{p=0}^{m-1} \sum_{r=0}^p C_p^r \frac{(a_1 + a_2)^{p-r} (a_3 P_r)^r}{\Gamma(m) m^r p!} \left(\frac{m \gamma_{SIC}}{P_c} \right)^p \exp \left(-\frac{m \gamma_{SIC} (a_1 + a_2)}{P_c} \right) \times \left(\frac{\gamma_{SIC} a_3 P_r}{P_c} + 1 \right)^{-(r+m)} \Gamma \left(r+m, \frac{\gamma_{th} m (a_4 + a_5)}{P_r} \left(\frac{\gamma_{SIC} a_3 P_r}{P_c} + 1 \right) \right), \quad (26)$$

where we have $a_4 = \frac{P_{BS} G_r C_r (d_r)^{-\alpha_r} \gamma^2 \beta_{semi}^2 B^2 \sigma_r^2}{G_c C_c (d_r)^{-\alpha_c}}$ and $a_5 = \frac{\sigma^2}{G_c C_c (d_r)^{-\alpha_c}}$.

Sketch of Proof: See Appendix B.

Corollary 3. In Scenario-I, the ergodic rate expression for the communication signal of the radar

target is

$$R_r^{er,I} = \frac{1}{\ln 2} \sum_{p=0}^{m-1} \sum_{r=0}^p C_p^r \frac{(a_1 + a_2)^{p-r} (a_3 P_r)^r}{\Gamma(m) m^r p!} \left(\frac{m \gamma_{SIC}}{P_c} \right)^p \exp(-\Lambda_1 \gamma_{SIC}) \left(\frac{\gamma_{SIC} a_3 P_r}{P_c} + 1 \right)^{-(r+m)} \\ \times \sum_{k=0}^{r+m-1} \frac{(r+m-1)! \Lambda_2}{k!} \exp(\Lambda_2) \Gamma(k+1) E_{1+k}(\Lambda_2), \quad (27)$$

where we have $\Lambda_2 = \frac{m(a_4+a_5)}{P_r} \left(\frac{\gamma_{SIC} a_3 P_r}{P_c} + 1 \right)$.

Sketch of Proof: The proof is similar to that of **Theorem 1**.

B. Performance Analysis for Communication Signals in Scenario-II

This subsection evaluates both the OP and the ergodic rate of NOMA-based Semi-ISaC in Scenario-II. Compared to Scenario-I, the SIC detection orders are the opposite way round. Thus, the OP expressions become

$$\mathbb{P}_r^{II} = \Pr \{ \gamma_r^{II} < \gamma_{th} \}, \quad (28)$$

$$\mathbb{P}_c^{II} = 1 - \Pr \{ \gamma_r^{II} > \gamma_{SIC}, \gamma_c^{II} > \gamma_{th} \}, \quad (29)$$

and the expressions of the OP and of the ergodic rate are presented by **Theorem 5-6** and **Corollary 4-5**.

Theorem 5. For NOMA-based Semi-ISaC in Scenario-II, the OP for the communication signal of the radar target is formulated as:

$$\mathbb{P}_r^{II} = 1 - \sum_{p=0}^{m-1} \sum_{r=0}^p \frac{C_p^r \Gamma(m+r)}{\Gamma(m) m^r p!} \left(\frac{m \gamma_{th}}{P_r} \right)^p \exp \left(-\frac{m \gamma_{th} (b_1 + b_2)}{P_r} \right) \\ \times (b_1 + b_2)^{p-r} (P_c b_3)^r \left(\frac{\gamma_{th} P_c b_3}{P_r} + 1 \right)^{-(m+r)}, \quad (30)$$

where we have $b_1 = \frac{P_{BS} G_r C_r \gamma^2 \beta_{semi}^2 B^2 \sigma_r^2}{G_c C_c (d_r)^{\alpha_r - \alpha_c}}$, $b_2 = \frac{\sigma^2}{G_c C_c (d_r)^{-\alpha_c}}$, $b_3 = \frac{(d_c)^{-\alpha_c}}{(d_r)^{-\alpha_c}}$.

Sketch of Proof: By the accurate series expansion for the lower incomplete Gamma function

and the binomial theorem, the OP expression is formulated as:

$$\mathbb{P}_r^{II} = 1 - \sum_{p=0}^{m-1} \frac{1}{p!} \left(\frac{m\gamma_{th}}{P_r} \right)^p \exp \left(-\frac{m\gamma_{th}(b_l + b_2)}{P_r} \right) \sum_{r=0}^p C_p^r (b_l + b_2)^{p-r} (P_c b_3)^r \times \underbrace{\int_0^\infty x^r \exp \left(-\frac{m\gamma_{th} P_c b_3}{P_r} x \right) f_{|h_c|^2}(x) dx}_{I_2}. \quad (31)$$

Furthermore, according to Eq. [2.3.3.1] in [34], we obtain the final analytical form. Additionally, the detailed proof is similar to that of **Theorem 3**.

Corollary 4. We define a parameter of $\Lambda_3 = \frac{m(b_l + b_2)}{P_r}$. In Scenario-II of the NOMA-based Semi-ISaC, the ergodic rate of the communication signal for the radar target is

$$R_r^{er,II} = \frac{1}{\ln 2} \sum_{p=0}^{m-1} \sum_{r=0}^p \sum_{k=0}^\infty \binom{m+r+k-1}{k} \frac{C_p^r \Gamma(m+r) \Gamma(p+k+1)}{\Gamma(m) m^r p! (b_l + b_2)^r \Lambda_3^{k+1}} \times (P_c b_3)^r \left(-\frac{P_c b_3}{P_r} \right)^k \exp(\Lambda_3) E_{p+k+1}(\Lambda_3). \quad (32)$$

Sketch of Proof: The proof is similar to that of **Corollary 2**.

Theorem 6. For the communication signal of the communication transmitter in the NOMA-based Semi-ISaC scenario, the OP expression is formulated as:

$$\mathbb{P}_c^{II} = 1 - \sum_{p=0}^{m-1} \frac{1}{p!} \left(\frac{m\gamma_{SIC}}{P_r} \right)^p \exp \left(-\frac{m\gamma_{SIC}(b_l + b_2)}{P_r} \right) \sum_{r=0}^p C_p^r (b_l + b_2)^{p-r} (P_c b_3)^r I_3, \quad (33)$$

where I_3 is given by

$$I_3 = \frac{1}{\Gamma(m) m^r} \left(\frac{\gamma_{SIC}}{P_r} P_c b_3 + 1 \right)^{-(m+r)} \Gamma \left(m+r, \frac{\gamma_{th} m}{P_c} (a_1 + a_2) \left(\frac{\gamma_{SIC}}{P_r} P_c b_3 + 1 \right) \right). \quad (34)$$

Sketch of Proof: By exploiting the series expansion of the incomplete Gamma function, the binomial theorem, and some equation manipulations, the OP of the communication transmitter in Scenario-II is

$$\mathbb{P}_c^{II} = 1 - \sum_{p=0}^{m-1} \frac{1}{p!} \left(\frac{m\gamma_{SIC}}{P_r} \right)^p \exp \left(-\frac{m\gamma_{SIC}(b_l + b_2)}{P_r} \right) \sum_{r=0}^p C_p^r (b_l + b_2)^{p-r} (P_c b_3)^r \times \underbrace{\int_{\frac{\gamma_{th}}{P_c}(a_1+a_2)}^\infty x^r \exp \left(-\frac{m\gamma_{SIC}}{P_r} P_c b_3 x \right) f_{|h_c|^2}(x) dx}_{I_3}. \quad (35)$$

Then, we can derive the final OP expression by substituting Eq. [2.3.6.6] from [34] into the expression as Eq. (35). The detailed proof is similar to that of **Theorem 4**.

Corollary 5. For Scenario-II, the ergodic rate expression of the communication signal for the communication transmitter is formulated as:

$$R_c^{er,II} = \frac{1}{\ln 2} \sum_{p=0}^{m-1} \sum_{r=0}^p \frac{C_p^r (P_c b_3)^r \Lambda_5^p \exp(-\Lambda_5)}{p! \Gamma(m) m^r (b_1 + b_2)^r} \left(\frac{\gamma_{SIC}}{P_r} P_c b_3 + 1 \right)^{-(m+r)} \\ \times \sum_{k=0}^{m+r-1} \frac{(m+r-1)!}{k! \Lambda_4} \exp(\Lambda_4) \Gamma(k+1) E_{k+1}(\Lambda_4), \quad (36)$$

where we have $\Lambda_4 = \frac{m}{P_c} (a_1 + a_2) \left(\frac{\gamma_{SIC}}{P_r} P_c b_3 + 1 \right)$ and $\Lambda_5 = \frac{m \gamma_{SIC} (b_1 + b_2)}{P_r}$.

Sketch of Proof: The proof is similar to that of **Corollary 2**.

C. Analytical Performance Evaluation for Radar Echoes

As the radar echoes are simply left behind after the last SIC process, the definition of ergodic RIER is the same as the OMA-based Semi-ISaC scenario when the SIC processes are successful. That is, under a perfect SIC case, the derivations of the ergodic REIR in the NOMA-based Semi-ISaC scenario are the same as those in the OMA-based Semi-ISaC scenario of **Theorem 1**. Hence, we will not repeat the derivations here. To gain further insights, the closed-form asymptotic expressions of the ergodic REIR are derived and evaluated in the next section.

V. ASYMPTOTIC PERFORMANCE EVALUATION FOR NOMA-BASED SEMI-ISAC

In this section, we derive the asymptotic OP and the ergodic REIR for further evaluating the performance of the NOMA-based Semi-ISaC system in the high-SNR region. We derive the diversity orders of the OP (for the communication signals) and present our insights in **Remark 1-5**. Additionally, we derive the high-SNR slopes of the ergodic REIR (for the radar echoes) and summarize them in **Remark 6-7**.

A. Asymptotic Outage Performance and Diversity Gains for Communication Signals

Recall that we consider two scenarios, namely Scenario-I having a near communication transmitter and a far radar target and Scenario-II associated with a far communication transmitter and a near radar target.

1) *Diversity Evaluation in Scenario-I:* Based on **Theorem 3** and **Theorem 4**, we evaluate the performance in the high-SNR region. Explicitly, we exploit the asymptotic series of the lower incomplete Gamma function and retain only a single term as the following form of

$$\gamma(a, b) \approx \sum_{n=0}^{\infty} \frac{(-1)^n b^{a+n}}{n! (a+n)} \approx \frac{b^a}{a}. \quad (37)$$

Then, we substitute Eq. (37) into the results of **Theorem 3** and **Theorem 4**, and following some further manipulations, we arrive at the asymptotic OP expressions, which are presented in **Corollary 6** and **Corollary 7**.

Corollary 6. For the communication signal of the communication transmitter in Scenario-I, the asymptotic OP expression is

$$\mathbb{P}_{c,\infty}^I = \left(\frac{m\gamma_{th}}{P_c} \right)^m \sum_{r=0}^m C_m^r (a_1 + a_2)^{m-r} \frac{(P_r a_3)^r \Gamma(m+r)}{\Gamma(m+1) \Gamma(m) m^r}. \quad (38)$$

Sketch of Proof: Upon Substituting Eq. (37) into the OP expression of **Theorem 3**, we arrive at

$$\mathbb{P}_{c,\infty}^I = \left(\frac{m\gamma_{th}}{P_c} \right)^m \sum_{r=0}^m C_m^r (a_1 + a_2)^{m-r} \frac{(P_r a_3)^r}{\Gamma(m+1)} \int_0^{\infty} x^r f_{|h_r|^2}(x) dx. \quad (39)$$

With the aid of the PDF of the Gamma distribution, we derive the integral as $\int_0^{\infty} x^r f_{|h_r|^2}(x) dx = \frac{m^m}{\Gamma(m)} \int_0^{\infty} x^{m+r-1} \exp(-mx) dx = \frac{\Gamma(m+r)}{\Gamma(m) m^r}$. Then, after we substitute the integral into the OP expression, this proof is completed.

Remark 1. We assume that the transmit power of the communication transmitter is increased to infinity for evaluating the outage performance in the high-SNR region. Thus, we can express the diversity order of the communication transmitter in Scenario-I as:

$$D_c^I = - \lim_{P_c \rightarrow \infty} \frac{\log(\mathbb{P}_{c,\infty}^I)}{\log(P_c)} = m, \quad (40)$$

which is proved by $\lim_{x \rightarrow \infty} \frac{\log[(A/x)^m]}{\log(x)} = m$ for a constant A independent of the variable x .

Corollary 7. For the communication signal of the radar target in Scenario-I, the asymptotic OP

is formulated as:

$$\mathbb{P}_{r,\infty}^I = F_{|h_r|^2} \left(\frac{\gamma_{th}(a_4 + a_5)}{P_r} \right) + \left(\frac{m\gamma_{SIC}}{P_c} \right)^m \sum_{r=0}^m C_m^r \frac{(a_3 P_r)^r \Gamma \left(m + r, \frac{m\gamma_{th}(a_4 + a_5)}{P_r} \right)}{(a_1 + a_2)^{r-m} \Gamma(m+1) \Gamma(m) m^r}. \quad (41)$$

Sketch of Proof: With the aid of **Theorem 4**, we can formulate the OP expression as:

$$\mathbb{P}_{r,\infty}^I = F_{|h_r|^2} \left(\frac{\gamma_{th}(a_4 + a_5)}{P_r} \right) + \left(\frac{m\gamma_{SIC}}{P_c} \right)^m \sum_{r=0}^m C_m^r \frac{(a_3 P_r)^r \int_{\frac{\gamma_{th}(a_4 + a_5)}{P_r}}^{\infty} x^r f_{|h_r|^2}(x) dx}{(a_1 + a_2)^{r-m} \Gamma(m+1)}, \quad (42)$$

and based on the PDF of the Gamma distribution and the integral $\frac{m^m}{\Gamma(m)} \int_{\frac{\gamma_{th}(a_4 + a_5)}{P_r}}^{\infty} x^{m+r-1} \times \exp(-mx) dx = \frac{1}{\Gamma(m)m^r} \Gamma \left(m + r, \frac{m\gamma_{th}(a_4 + a_5)}{P_r} \right)$, the final OP expression is derived.

Remark 2. Under the same assumption as in **Remark 1**, based on the asymptotic expression of the radar target's communication signal, we derive the diversity order for the radar target in Scenario-I as:

$$D_r^I = - \lim_{P_c \rightarrow \infty} \frac{\log(\mathbb{P}_{r,\infty}^I)}{\log(P_c)} = 0, \quad (43)$$

which is proved by $\lim_{x \rightarrow \infty} \frac{\log[(A/x)^m + B]}{\log(x)} = 0$ with the constants A and B being independent of the variable x .

2) *Diversity Evaluation in Scenario-II:* For Scenario-II of the NOMA-based Semi-ISaC network, based on the results of **Theorem 5** and **Theorem 6**, we are able to exploit the asymptotic series expansion of Eq. (37) for deriving the asymptotic OP. Thus, the asymptotic OP of the communication transmitter and radar target are given by **Corollary 8** and **Corollary 9**, respectively.

Corollary 8. In Scenario-II, the asymptotic OP expression of the communication transmitter is

$$\mathbb{P}_{c,\infty}^{II} = F_{|h_c|^2} \left(\frac{\gamma_{th}}{P_c} (a_1 + a_2) \right) + \left(\frac{m\gamma_{SIC}}{P_r} \right)^m \sum_{r=0}^m C_m^r \frac{(P_c b_3)^r \Gamma \left(m + r, \frac{m\gamma_{th}}{P_c} (a_1 + a_2) \right)}{(b_1 + b_2)^{r-m} \Gamma(m+1) \Gamma(m) m^r}. \quad (44)$$

Sketch of Proof: The proof is similar to that of **Corollary 7**.

Remark 3. In Scenario-II, we evaluate the outage performance in the high-SNR region by assuming that the transmit power of the radar target is infinity. Based on the **Corollary 8**, the

diversity order of the communication transmitter is expressed as:

$$D_c^{II} = - \lim_{P_r \rightarrow \infty} \frac{\log(\mathbb{P}_{c,\infty}^{II})}{\log(P_r)} = 0. \quad (45)$$

Corollary 9. In Scenario-II, the asymptotic OP expression of the radar target is derived as:

$$\mathbb{P}_{r,\infty}^{II} = \left(\frac{m\gamma_{th}}{P_r} \right)^m \sum_{r=0}^m C_m^r (b_l + b_2)^{m-r} \frac{(P_c b_3)^r \Gamma(m+r)}{\Gamma(m+1) \Gamma(m) m^r}. \quad (46)$$

Sketch of Proof: The proof is similar to that of Corollary 6.

Remark 4. Under the same assumptions as in **Remark 3**, we exploit the asymptotic expressions yielding the diversity order of the communication signal of the radar target in Scenario-II as:

$$D_r^{II} = - \lim_{P_r \rightarrow \infty} \frac{\log(\mathbb{P}_{r,\infty}^{II})}{\log(P_r)} = m. \quad (47)$$

Remark 5. For Nakagami- m fading channels, the higher the parameter m , the stronger the LoS component becomes. Hence, we conclude that for high LoS components, we have high diversity orders, yielding a Neal-Gaussian performance reminiscent of asymptotically infinite diversity order.

B. Asymptotic Ergodic REIR and High-SNR Slopes

To gain further insights, we exploit the asymptotic expansions of the lower incomplete Gamma function and the generalized exponential integral to derive the asymptotic ergodic REIR for the radar target, expressed as $\gamma(m, t) = (m-1)! - \exp(-t) \sum_{k=0}^{m-1} \frac{(m-1)!}{k!} t^k$, $E_n(z) \approx \frac{(-z)^{n-1}}{(n-1)!} (\psi(n) - \ln(z)) - \sum_{k=0 \& k \neq n-1} \frac{(-z)^k}{k!(1-n+k)}$ for $n > 1$, and $E_1(z) \approx -C_\gamma - \ln(z) + z$, where C_γ is the Euler constant and $\psi(n)$ is the Psi function. Thus, the asymptotic expression of the ergodic REIR for radar target is given in **Corollary 10**. Additionally, with the aid of the closed-form asymptotic expression, we can evaluate the high-SNR slope, which will be derived in **Remark 6**.

Corollary 10. Upon assuming that m is an integer denoted as $m \in \mathbb{Z}$, we derive the closed-form asymptotic expression of the ergodic REIR, which will be derived in the following form of

$$R_{est}^\infty = \frac{\delta m^m}{2T \ln(2) \Gamma(m)} I_4 + \sum_{k=l}^{m-1} \frac{\delta m^m}{2T \ln(2) \Gamma(m)} I_5, \quad (48)$$

where I_4 and I_5 are formulated as:

$$I_4 = \frac{d_t^{\alpha_r} \Gamma(m-1)}{\Xi_{r,1} m^{m-2}} - \frac{\Gamma(m)}{m^m} \left(\log \left(\frac{m^2 d_t^{\alpha_r}}{\Xi_{r,1}} \right) - \psi^{(0)}(m) - C_\gamma \right) \\ + \left(\frac{m d_t^{\alpha_r}}{\Xi_{r,1}} \right)^2 \frac{\Gamma(m-2)}{m^{m-2}} - \frac{m d_t^{\alpha_r}}{\Xi_{r,1}} \frac{\Gamma(m-1)}{m^{m-1}} \left(\log \left(\frac{m^2 d_t^{\alpha_r}}{\Xi_{r,1}} \right) - \psi^{(0)}(m-1) - C_\gamma \right), \quad (49)$$

$$I_5 = \left(-\frac{d_t^{\alpha_r}}{\Xi_{r,1}} \right)^k \frac{\psi(k+1) \Gamma(m-k)}{k! m^m} + \sum_{q=0 \& q \neq k}^{m-1} \frac{\Gamma(m-q) \left(-\frac{m d_t^{\alpha_r}}{\Xi_{r,1}} \right)^q}{q! (q-k) m^{m-q}} \\ - \frac{\Gamma(m-k)}{m^{m-k} k!} \left(-\frac{m d_t^{\alpha_r}}{\Xi_{r,1}} \right)^k \left(\ln \left(\frac{m^2 d_t^{\alpha_r}}{\Xi_{r,1}} \right) - \psi^{(0)}(m-k) \right). \quad (50)$$

Sketch of Proof: See Appendix C.

Based on the above asymptotic closed-form expressions, we can evaluate the high-SNR slope of the radar target. When the transmit power of the BS is increased as $P_{BS} \rightarrow \infty$, the high-SNR slope is defined as:

$$S = \lim_{P_{BS} \rightarrow \infty} \frac{R_{est,\infty}^{low}(P_{BS})}{\ln(P_{BS})}. \quad (51)$$

Remark 6. Upon substituting the expression in **Corollary 10** into Eq. (51), the high-SNR slope may be formulated as:

$$S = \lim_{P_{BS} \rightarrow \infty} \frac{\frac{\delta m^m}{2T \ln(2) \Gamma(m)} I_7}{\ln(P_{BS})} + \lim_{P_{BS} \rightarrow \infty} \frac{\frac{\delta m^m}{2T \ln(2) \Gamma(m)} I_8}{\ln(P_{BS})} = \frac{\delta}{2T \ln(2)}, \quad (52)$$

which is proved by exploiting $\lim_{P_{BS} \rightarrow \infty} \frac{\left(\frac{A}{P_{BS}} \right)^k - B \ln \left(\frac{C}{P_{BS}} \right) + D}{\ln(P_{BS})} = B$ and $\lim_{P_{BS} \rightarrow \infty} \frac{\left(\frac{A}{P_{BS}} \right)^k}{\ln(P_{BS})} - \frac{\left(\frac{B}{P_{BS}} \right)^k \ln \left(\frac{C}{P_{BS}} \right)}{\ln(P_{BS})} + \frac{D}{\ln(P_{BS})} = 0$, where A , B , C , and D are constants that are independent of the variable P_{BS} .

Remark 7. The high-SNR slope is only influenced by the radar's duty cycle δ and the pulse duration T . Additionally, the high-SNR slope is proportional to δ/T .

VI. NUMERICAL RESULTS

Our numerical analysis is presented in this section, where the parameters are set as: the distance of the near-user is 800 meter and that of the far-user is 1300 meter, the bandwidth is $B = 10$ MHz, the noise power is $\sigma^2 = k_b B T_{temp}$ with $T_{temp} = 724$ K, the target rates of the wireless communications are $\hat{R}_{OMA} = \hat{R}_{NOMA} = 1$ given the thresholds $\gamma_{th} = 2^{\hat{R}_{NOMA}} - 1$ for NOMA and $\gamma_{th}^{OMA} = 2^{\hat{R}_{OMA}} - 1$ for OMA, the threshold for SIC is $\gamma_{SIC} = 0.4$, the carrier

frequency is $f_c = 10^9$ Hz, the speed of light is $c = 3 \times 10^8$ m/s, the target radar cross section is $\sigma_{RCS} = 0.1$, the pulse duration is $T = 1 \mu\text{s}$, the path loss exponents are $\alpha_r = 4.5$ and $\alpha_c = 2.5$, the radar's duty cycle is $\delta = 0.01$, and the Nakagami coefficient is $m = 3$. We define the average received SINR as $\mathbb{E} [P_t |h|^2 C_j d^{-\alpha_j} / \sigma^2]$ (dB) where we exploit the subscript of $j \in \{c, r\}$ for representing the communication channels or the radar detection channels.

A. From OMA-based Semi-ISaC to NOMA-based Semi-ISaC

In Fig. 2(a), we quantity the OP and the ergodic rate (with the unit as *bit per cell use*, denoted as BPCU) versus the received power level (with the distance as $d = 800$ meters) of the OMA user under the OMA-based Semi-ISaC scenario. We observe that the analytical results are closely matched by the simulation results. In Fig. 2(b), we investigate the performance interplay between the radar signals and wireless communications for $\beta_{semi} \in [0, 1]$ when we set $\alpha_{semi} = 0$ and $\epsilon_{semi} = 1 - \beta_{semi}$. We then set the transmit power is 10 dBm for both users and the BS. Additionally, we compare the performance among conventional (FD) ISaC, OMA-based Semi-ISaC, and NOMA-based Semi-ISaC networks and thus observe that Semi-ISaC has better channel capacity than the conventional ISaC. The reason is that for Semi-ISaC, radar and communication signals share the same resource blocks in ISaC bandwidth with the aid of SIC to obtain better BE than the conventional ISaC. Another conclusion is that the NOMA-based Semi-ISaC scenario has a higher capacity than its OMA-based Semi-ISaC counterpart because the BE is enhanced by the NOMA technique. Additionally, the ergodic REIR (for radar signals) is zero when we have $\beta_{semi} = 0$ because all the bandwidth is used for wireless communication and no bandwidth is set aside for radar estimation. Upon considering $\beta_{semi} = 1$, we have the highest ergodic REIR, while the ergodic rate (for communication signals) cannot be reduced to zero. This represents the ISaC scenario (not Semi-ISaC), where the total bandwidth is utilized both for radar estimation and for wireless communication.

B. Outage Probability for Communication Signals in NOMA-based Semi-ISaC

Let us now validate the analytical and asymptotic OP expressions of NOMA users in Fig. 3(a) and Fig. 3(b). Explicitly, in Fig. 3(a), a close communication transmitter ($d_c = \{500, 800\}$ meter) and a distant radar target ($d_r = \{800, 1000\}$ meter) are considered as Scenario-I. By contrast, in Fig. 3(b), our Scenario-II of a distant communication transmitter ($d_c = \{800, 1000\}$ meter) and a close radar target ($d_r = \{500, 800\}$ meter) is considered. The simulation results closely match the

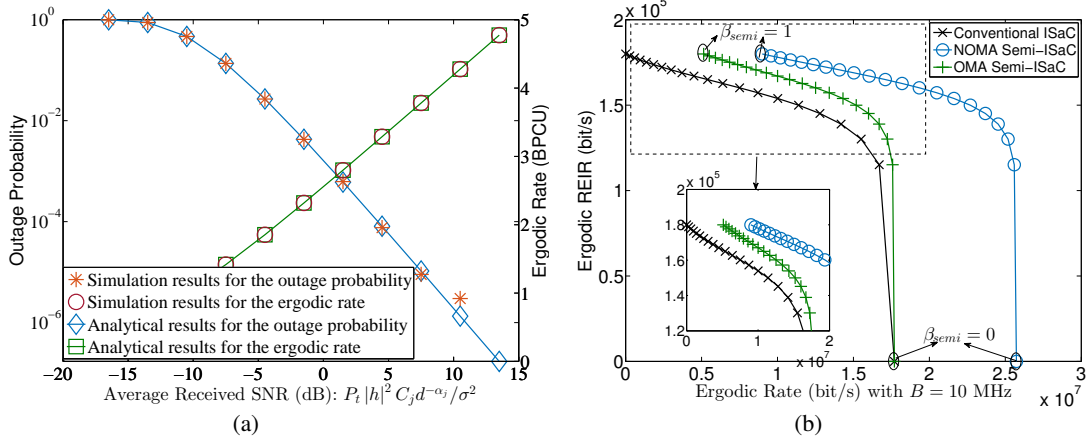


Fig. 2. From OMA to NOMA: (a) The verification of the OP and the ergodic rate for the OMA-based Semi-ISaC system based on **Theorem 1-2**; (b) A comparison among the conventional (FD) ISaC, OMA-based Semi-ISaC, and NOMA-based Semi-ISaC and the interplay between the radar target (ergodic REIR) and the communication transmitter (ergodic rate) with various $\beta_{semi} \in [0, 1]$.

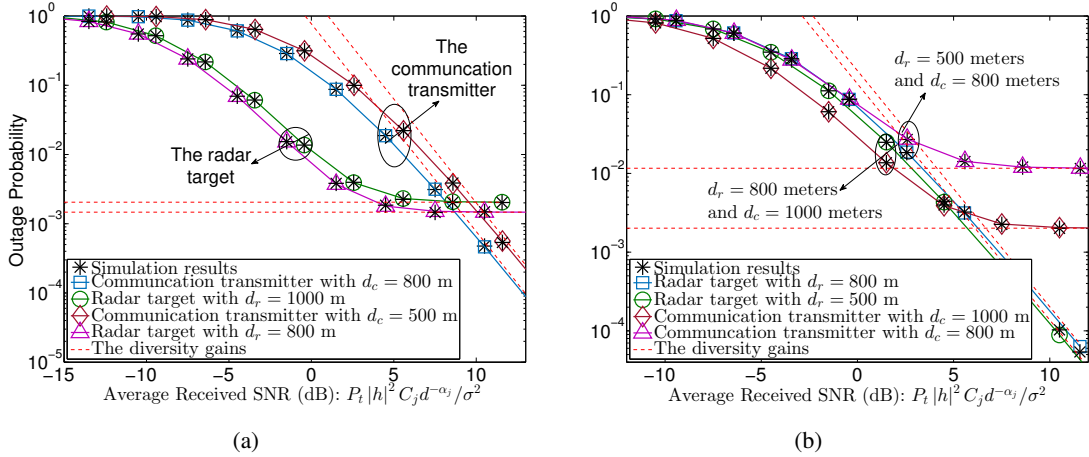


Fig. 3. Outage performance: (a) OP versus the received SNR of the communication transmitter in Scenario-I; (b) OP versus the received SNR of the radar target in Scenario-II. The analytical results are based on **Theorem 3-6**, **Corollary 2-9**, and **Remark 1-5**.

analytical results and the diversity analysis matches the OP performance in the high-SNR region. A conclusion for both scenarios is that upon increasing the near-user's received SNR, the OP of both users will be reduced, but the far-user will enhance an OP floor. This is because for the near-user, enhancing its received SNR directly increases the signal strength, hence resulting in the reduced OP. By contrast, for the far-user, enhancing the near-user's received SNR beneficially improves the error rate of SIC, which only improves the OP of the distant user to a lower limit. But once the SIC process becomes perfect, the lower OP limit is reached.

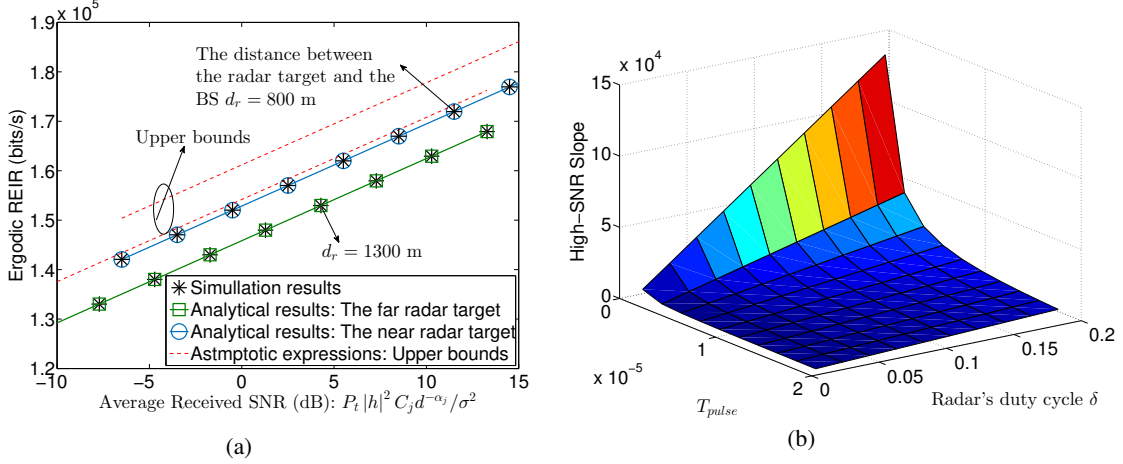


Fig. 4. The ergodic REIR: (a) The ergodic REIR versus the received SNR of the BS with various distance $d_r = [800, 1300]$ meters; (b) The ergodic REIR varies based on different value of the radar's duty cycle δ and the pulse duration T . The analytical results are based on **Theorem 2**, **Corollary 10**, and **Remark 6-7**.

C. Ergodic REIR for Radar Echoes in NOMA-based Semi-ISaC

In Fig. 4(a), the ergodic REIR of NOMA users is quantified. The analytical results fit the simulation results well and the asymptotic results represent the upper bound of the simulation results. Based on **Remark 6**, the high-SNR slope is influenced by the ratio of the radar's duty cycle and pulse duration (δ/T). Thus, in Fig. 4(b), we investigate how the radar's duty cycle and the pulse duration influence the ergodic REIR. Firstly, it is indicated in Fig. 4(b) that the user having a higher radar's duty cycle has a better ergodic REIR, since increasing the radar's duty cycle requires us to increase the radar pulse duration in the same period. Additionally, it is concluded that for the same radar's duty cycle, the user having lower pulse duration has a better ergodic REIR. This is because when the radar's duty cycle is fixed, reducing the pulse duration reduces the time between two pulses, thus the density of pulses is increased.

VII. CONCLUSIONS

We have proposed the Semi-ISaC networking concept, where the total bandwidth is split into three portions, i.e., the communication-only bandwidth, the radar-echo-only bandwidth, and the ISaC bandwidth. When detecting the communication signals in the ISaC band, we consider the radar echo as interference contaminating the communication signals. We have then evolved our novel Semi-ISaC concept from OMA-based Semi-ISaC to NOMA-based Semi-ISaC. We have then characterized the novel ergodic REIR metric for quantifying the average radar estimation rate. We have derived the OP and the ergodic rate for the communication signals and the ergodic RIER for the radar echo in the OMA-based Semi-ISaC scenario. Additionally, we have evaluated

the performance in the NOMA-based Semi-ISaC scenario. More specifically, we have derived the analytical expressions of the OP and the ergodic rate for communication signals. We have also derived the asymptotic OP along with the diversity gains attained for communication signals. Moreover, for the radar echo, we have derived the analytical expressions of the ergodic REIR, followed by the asymptotic ergodic REIR along with the high-SNR slopes. Our analysis has confirmed that: 1) The channel capacity of the conventional ISaC is lower than that of Semi-ISaC. 2) NOMA-based Semi-ISaC has better capacity than OMA-based Semi-ISaC; 3) The diversity gain of the communication signal is determined by the power of the line-of-sight component m ; and 4) We can strike a flexible trade-off by balancing the radar and communication signals upon jointly controlling the transmit power of the BS, the radar's duty cycle, and the pulse duration.

APPENDIX A: PROOF OF THEOREM 3

For deriving the closed-form OP expressions for the communication transmitter, the probability expression should be manipulated as follows:

$$\mathbb{P}_c^I = \Pr \{ \gamma_c^I < \gamma_{th} \} = \Pr \left\{ |h_c|^2 < \frac{\gamma_{th} P_r |h_r|^2 (d_r)^{-\alpha_c}}{P_c (d_c)^{-\alpha_c}} + \frac{\gamma_{th} \mathbb{E}[I_R] (d_r) + \gamma_{th} \sigma^2}{P_c G_c C_c (d_c)^{-\alpha_c}} \right\}. \quad (\text{A.1})$$

Upon substituting the expectation of interference in **Lemma 1** and rewriting the probability equation in form of integrals, we present the OP expression by exploiting the PDF and CDF of the Nakagami- m fading channels as follows:

$$\mathbb{P}_c^I = \int_0^\infty \frac{1}{\Gamma(m)} \gamma \left(m, m \left(\frac{\gamma_{th} P_r x (d_r)^{-\alpha_c}}{P_c (d_c)^{-\alpha_c}} + \frac{\gamma_{th} \mathbb{E}[I_R] (d_r) + \gamma_{th} \sigma^2}{P_c G_c C_c (d_c)^{-\alpha_c}} \right) \right) f_{|h_r|^2}(x) dx. \quad (\text{A.2})$$

Since the CDF of the Nakagami- m fading channel (in power domain) is a lower incomplete Gamma function, the accurate series expansion of the incomplete Gamma function may be exploited for reducing the complexity of derivation, which is expressed as:

$$\gamma(a, b) = \Gamma(a) - \Gamma(a, b) = \Gamma(a) - \sum_{p=0}^{a-1} \frac{(a-1)!}{p!} \exp(-b) b^p, \quad (\text{A.3})$$

where $\Gamma(a, b)$ is the upper incomplete Gamma function.

By substituting this equation into Eq. (A.2), we obtain the further streamlined expressions of

$$\begin{aligned} \mathbb{P}_c^I = & 1 - \exp\left(-\frac{m\gamma_{th}}{P_c}(a_1 + a_2)\right) \sum_{p=0}^{m-1} \frac{(m\gamma_{th})^p}{p!} \\ & \times \int_0^\infty \exp\left(-\frac{m\gamma_{th}P_r a_3}{P_c}x\right) \left(\frac{P_r a_3 x}{P_c} + \frac{a_1 + a_2}{P_c}\right)^p f_{|h_r|^2}(x) dx. \end{aligned} \quad (\text{A.4})$$

The former expression Eq. (A.4) is then formulated with the aid of the Binomial theorem as:

$$\begin{aligned} \mathbb{P}_c^I = & 1 - \exp\left(-\frac{m\gamma_{th}}{P_c}(a_1 + a_2)\right) \sum_{p=0}^{m-1} \frac{(m\gamma_{th})^p}{p!} \sum_{r=0}^p C_p^r \frac{(a_1 + a_2)^r (P_r a_3)^{p-r}}{P_c^p} \\ & \times \int_0^\infty \exp\left(-\frac{m\gamma_{th}a_3 P_r}{P_c}x\right) x^{p-r} f_{|h_r|^2}(x) dx. \end{aligned} \quad (\text{A.5})$$

We now exploit Eq. [2.3.3.1] of [34] to obtain Eq. (23). Then, the proof is completed.

APPENDIX B: PROOF OF THEOREM 4

The OP for the radar target under the NOMA-based Semi-ISaC scenario is expressed as:

$$\mathbb{P}_r^I = 1 - \Pr\left\{|h_c|^2 > \gamma_{SIC} \frac{a_3 P_r |h_r|^2 + a_1 + a_2}{P_c}, |h_r|^2 > \frac{\gamma_{th}(a_4 + a_5)}{P_r}\right\}. \quad (\text{B.1})$$

Substituting the CDF of the Nakagami- m fading channels into Eq. (B.1), the resultant probability expression can be further transformed to

$$\mathbb{P}_r^I = 1 - \int_{\frac{\gamma_{th}(a_4 + a_5)}{P_r}}^\infty \left(1 - \frac{1}{\Gamma(m)} \gamma\left(m, \frac{m\gamma_{SIC}}{P_c} (a_3 P_r |h_r|^2 + a_1 + a_2)\right)\right) f_{|h_r|^2}(x) dx. \quad (\text{B.2})$$

By exploiting an accurate series expansion of the lower incomplete Gamma function, and then further manipulating the equations, the OP expression is derived as:

$$\begin{aligned} \mathbb{P}_r^I = & 1 - \sum_{p=0}^{m-1} \frac{1}{p!} \left(\frac{m\gamma_{SIC}}{P_c}\right)^p \exp\left(-\frac{m\gamma_{SIC}(a_1 + a_2)}{P_c}\right) \sum_{r=0}^p C_p^r (a_1 + a_2)^{p-r} (a_3 P_r)^r \\ & \times \underbrace{\int_{\frac{\gamma_{th}(a_4 + a_5)}{P_r}}^\infty \exp\left(-\frac{m\gamma_{SIC}a_3 P_r x}{P_c}\right) x^r f_{|h_r|^2}(x) dx}_{I_1}. \end{aligned} \quad (\text{B.3})$$

Then we can derive I_1 based on Eq. [2.3.6.6] of [34], yielding:

$$I_1 = \frac{1}{\Gamma(m) m^r} \left(\frac{\gamma_{SIC}a_3 P_r}{P_c} + 1\right)^{-(r+m)} \Gamma\left(r + m, \frac{\gamma_{th}m(a_4 + a_5)}{P_r} \left(\frac{\gamma_{SIC}a_3 P_r}{P_c} + 1\right)\right). \quad (\text{B.4})$$

Finally, upon substituting I_1 from Eq. (B.4) into the OP expression of Eq. (B.3), we can obtain the closed-form expression Eq. (26). This completes the proof.

APPENDIX C: PROOF OF COROLLARY 10

We first express the ergodic REIR with the aid of the following integrals as:

$$R_{est} \approx \sum_{k=0}^{m-1} \frac{\delta}{2T \ln(2)} \int_0^\infty \left(\frac{md_t^{\alpha_r}}{\Xi_{r,1}x} \right)^k \int_0^\infty \frac{1}{z+1} \exp\left(-\frac{md_t^{\alpha_r}}{\Xi_{r,1}x} z\right) \frac{z^k}{k!} dz f_{|h_{r,u}|^2}(x) dx. \quad (C.1)$$

With the aid of Eq. [2.3.6.9] of [34], we have

$$R_{est} \approx \sum_{k=0}^{m-1} \frac{\delta}{2T \ln(2)} \int_0^\infty \left(\frac{md_t^{\alpha_r}}{\Xi_{r,1}x} \right)^k \Psi\left(k+1, k+1, \frac{md_t^{\alpha_r}}{\Xi_{r,1}x}\right) f_{|h_{r,u}|^2}(x) dx, \quad (C.2)$$

and based on $\Psi(a, a, z) = z^{1-a} \exp(z) E_a(z)$, the expression above is further formulated as:

$$\begin{aligned} R_{est}^\infty &\approx \underbrace{\frac{\delta m^m}{2T \ln(2) \Gamma(m)} \int_0^\infty \left(1 + \frac{md_t^{\alpha_r}}{\Xi_{r,1}x}\right) x^{m-1} \exp(-mx) E_1\left(\frac{md_t^{\alpha_r}}{\Xi_{r,1}x}\right) dx}_{I_4} \\ &+ \underbrace{\sum_{k=1}^{m-1} \frac{\delta m^m}{2T \ln(2) \Gamma(m)} \int_0^\infty x^{m-1} \exp(-mx) \underbrace{E_{k+1}}_{P_{BS} \rightarrow \infty}\left(\frac{md_t^{\alpha_r}}{\Xi_{r,1}x}\right) dx}_{I_5}, \end{aligned} \quad (C.3)$$

where $\underbrace{E_{k+1}}_{P_{BS} \rightarrow \infty}\left(\frac{md_t^{\alpha_r}}{\Xi_{r,1}x}\right) \approx \frac{\left(-\frac{md_t^{\alpha_r}}{\Xi_{r,1}x}\right)^k}{k!} \left(\psi(k+1) - \ln\left(\frac{md_t^{\alpha_r}}{\Xi_{r,1}x}\right)\right) - \sum_{q=0 \& q \neq k}^{m-1} \frac{\left(-\frac{md_t^{\alpha_r}}{\Xi_{r,1}x}\right)^q}{q!(q-k)}$ for $k > 0$.

The equation I_4 is further formulated as:

$$I_4 = \underbrace{\int_0^\infty x^{m-1} \exp(-mx) E_1\left(\frac{md_t^{\alpha_r}}{\Xi_{r,1}x}\right) dx}_{I_6} + \underbrace{\frac{md_t^{\alpha_r}}{\Xi_{r,1}} \int_0^\infty x^{m-2} \exp(-mx) E_1\left(\frac{md_t^{\alpha_r}}{\Xi_{r,1}x}\right) dx}_{I_7}. \quad (C.4)$$

Based on the asymptotic expressions (expressed as $\gamma(m, t) = (m-1)! \exp(-t) \sum_{k=0}^{m-1} \frac{(m-1)!}{k!} t^k$, $E_n(z) \approx \frac{(-z)^{n-1}}{(n-1)!} (\psi(n) - \ln(z)) - \sum_{k=0 \& k \neq n-1} \frac{(-z)^k}{k!(1-n+k)}$ for $n > 1$, and $E_1(z) \approx -C_\gamma - \ln(z) + z$), I_6 and I_7 are derived as:

$$I_6 = \frac{d_t^{\alpha_r} \Gamma(m-1)}{\Xi_{r,1} m^{m-2}} - \frac{\Gamma(m)}{m^m} \left(\log\left(\frac{m^2 d_t^{\alpha_r}}{\Xi_{r,1}}\right) - \psi^{(0)}(m) - C_\gamma \right), \quad (C.5)$$

$$I_7 = \left(\frac{md_t^{\alpha_r}}{\Xi_{r,1}}\right)^2 \frac{\Gamma(m-2)}{m^{m-2}} - \frac{md_t^{\alpha_r}}{\Xi_{r,1}} \frac{\Gamma(m-1)}{m^{m-1}} \left(\log\left(\frac{m^2 d_t^{\alpha_r}}{\Xi_{r,1}}\right) - \psi^{(0)}(m-1) - C_\gamma \right). \quad (C.6)$$

Then, we can derive I_5 of Eq. (C.3) by substituting the asymptotic expressions of $E_{k+1} \left(\frac{md_t^{\alpha_r}}{\Xi_{r,1}x} \right)$, $P_{BS} \rightarrow \infty$. Finally, we can substitute I_4 and I_5 into (C.3) to obtain the final answer as Eq. (48).

REFERENCES

- [1] C. Zhang, W. Yi, and Y. Liu, "NOMA assisted ISaC networks with randomly deployed users," in *IEEE Proc. of International Commun. Conf. (ICC)*, 2022.
- [2] T. Wild, V. Braun, and H. Viswanathan, "Joint design of communication and sensing for beyond 5G and 6G systems," *IEEE Access*, vol. 9, pp. 30 845–30 857, 2021.
- [3] C. Sturm and W. Wiesbeck, "Waveform design and signal processing aspects for fusion of wireless communications and radar sensing," *Proc. IEEE*, vol. 99, no. 7, pp. 1236–1259, Jul. 2011.
- [4] J. A. Zhang, F. Liu, C. Masouros, R. W. Heath, Z. Feng, L. Zheng, and A. Petropulu, "An overview of signal processing techniques for joint communication and radar sensing," *IEEE J. Sel. Topics Signal Process.*, 2021, to be published.
- [5] A. Liu, Z. Huang, M. Li, Y. Wan, W. Li, T. X. Han, C. Liu, R. Du, D. T. K. Pin, J. Lu, Y. Shen, F. Colone, and K. Chetty, "A survey on fundamental limits of integrated sensing and communication," Apr. 2021, arXiv preprint arXiv:2104.09954. [Online]. Available: <https://arxiv.org/abs/2104.09954>
- [6] H. Griffiths, L. Cohen, S. Watts, E. Mokole, C. Baker, M. Wicks, and S. Blunt, "Radar spectrum engineering and management: Technical and regulatory issues," *Proc. of the IEEE*, vol. 103, no. 1, pp. 85–102, Jan. 2015.
- [7] Y. Liu, Z. Qin, M. ElKashlan, Z. Ding, A. Nallanathan, and L. Hanzo, "Nonorthogonal multiple access for 5G and beyond," *Proc. IEEE*, vol. 105, no. 12, pp. 2347–2381, Dec. 2017.
- [8] F. Liu, C. Masouros, A. P. Petropulu, H. Griffiths, and L. Hanzo, "Joint radar and communication design: Applications, state-of-the-art, and the road ahead," *IEEE Trans. Commun.*, vol. 68, no. 6, pp. 3834–3862, Jun. 2020.
- [9] A. R. Chiriyath, B. Paul, G. M. Jacyna, and D. W. Bliss, "Inner bounds on performance of radar and communications co-existence," *IEEE Trans. Signal Process.*, vol. 64, no. 2, pp. 464–474, Jan. 2016.
- [10] S. M. R. Islam, M. Zeng, O. A. Dobre, and K.-S. Kwak, "Resource allocation for downlink NOMA systems: Key techniques and open issues," *IEEE Wireless Commun.*, vol. 25, no. 2, pp. 40–47, Apr. 2018.
- [11] Y. Cui, F. Liu, X. Jing, and J. Mu, "Integrating sensing and communications for ubiquitous IoT: Applications, trends, and challenges," *IEEE Netw.*, vol. 35, no. 5, pp. 158–167, Sep. 2021.
- [12] Y. Liu, Z. Ding, M. ElKashlan, and H. V. Poor, "Cooperative non-orthogonal multiple access with simultaneous wireless information and power transfer," *IEEE J. Sel. Areas Commun.*, vol. 34, no. 4, pp. 938–953, Apr. 2016.
- [13] Z. Ding, R. Schober, and H. V. Poor, "Unveiling the importance of SIC in NOMA systems-part II: New results and future directions," *IEEE Commun. Lett.*, vol. 24, no. 11, pp. 2378–2382, Nov. 2020.
- [14] B. Xia, J. Wang, K. Xiao, Y. Gao, Y. Yao, and S. Ma, "Outage performance analysis for the advanced SIC receiver in wireless NOMA systems," *IEEE Trans. Veh. Technol.*, vol. 67, no. 7, pp. 6711–6715, Jul. 2018.
- [15] A. S. de Sena, F. R. M. Lima, D. B. da Costa, Z. Ding, P. H. J. Nardelli, U. S. Dias, and C. B. Papadias, "Massive MIMO-NOMA networks with imperfect SIC: Design and fairness enhancement," *IEEE Trans. Wireless Commun.*, vol. 19, no. 9, pp. 6100–6115, Sep. 2020.
- [16] W. Yi, Y. Liu, A. Nallanathan, and M. ElKashlan, "Clustered millimeter-wave networks with non-orthogonal multiple access," *IEEE Trans. Commun.*, vol. 67, no. 6, pp. 4350–4364, Jun. 2019.
- [17] L. Zhu, J. Zhang, Z. Xiao, X. Cao, D. O. Wu, and X.-G. Xia, "Joint power control and beamforming for uplink non-orthogonal multiple access in 5G millimeter-wave communications," *IEEE Trans. Wireless Commun.*, vol. 17, no. 9, pp. 6177–6189, Sep. 2018.
- [18] J. Cui, Y. Liu, Z. Ding, P. Fan, and A. Nallanathan, "Optimal user scheduling and power allocation for millimeter wave NOMA systems," *IEEE Trans. Wireless Commun.*, vol. 17, no. 3, pp. 1502–1517, Mar. 2018.
- [19] J. A. Mahal, A. Khawar, A. Abdelhadi, and T. C. Clancy, "Spectral coexistence of MIMO radar and MIMO cellular system," *IEEE Trans. Aerosp. Electron. Syst.*, vol. 53, no. 2, pp. 655–668, Apr. 2017.
- [20] B. Kang, O. Aldayel, V. Monga, and M. Rangaswamy, "Spatio-spectral radar beampattern design for coexistence with wireless communication systems," *IEEE Trans. Aerosp. Electron. Syst.*, vol. 55, no. 2, pp. 644–657, Apr. 2019.
- [21] F. Liu, L. Zhou, C. Masouros, A. Li, W. Luo, and A. Petropulu, "Toward dual-functional radar-communication systems: Optimal waveform design," *IEEE Trans. Signal Process.*, vol. 66, no. 16, pp. 4264–4279, Aug. 2018.
- [22] F. Wang and H. Li, "Power allocation for coexisting multicarrier radar and communication systems in cluttered environments," *IEEE Trans. Signal Process.*, vol. 69, pp. 1603–1613, 2021.
- [23] J. Qian, M. Lops, L. Zheng, X. Wang, and Z. He, "Joint system design for coexistence of MIMO radar and MIMO communication," *IEEE Trans. Signal Process.*, vol. 66, no. 13, pp. 3504–3519, Jul. 2018.

- [24] N. Cao, Y. Chen, X. Gu, and W. Feng, "Joint radar-communication waveform designs using signals from multiplexed users," *IEEE Trans. Commun.*, vol. 68, no. 8, pp. 5216–5227, Aug. 2020.
- [25] K. Wu, J. A. Zhang, X. Huang, Y. J. Guo, and R. W. Heath, "Waveform design and accurate channel estimation for frequency-hopping MIMO radar-based communications," *IEEE Trans. Commun.*, vol. 69, no. 2, pp. 1244–1258, Feb. 2021.
- [26] M. Temiz, E. Alsusa, and M. W. Baidas, "Optimized precoders for massive MIMO OFDM dual radar-communication systems," *IEEE Trans. Commun.*, vol. 69, no. 7, pp. 4781–4794, Jul. 2021.
- [27] K. Wu, J. A. Zhang, X. Huang, Y. J. Guo, and J. Yuan, "Reliable frequency-hopping MIMO radar-based communications with multi-antenna receiver," *IEEE Trans. Commun.*, vol. 69, no. 8, pp. 5502–5513, Aug. 2021.
- [28] F. Liu, C. Masouros, A. Li, T. Ratnarajah, and J. Zhou, "MIMO radar and cellular coexistence: A power-efficient approach enabled by interference exploitation," *IEEE Trans. Signal Process.*, vol. 66, no. 14, pp. 3681–3695, Jul. 2018.
- [29] L. Zheng, M. Lops, and X. Wang, "Adaptive interference removal for uncoordinated radar/communication coexistence," *IEEE J. Sel. Topics Signal Process.*, vol. 12, no. 1, pp. 45–60, Feb. 2018.
- [30] N. Nartasilpa, A. Salim, D. Tuninetti, and N. Devroye, "Communications system performance and design in the presence of radar interference," *IEEE Trans. Commun.*, vol. 66, no. 9, pp. 4170–4185, Sep. 2018.
- [31] F. Liu, C. Masouros, A. Li, H. Sun, and L. Hanzo, "MU-MIMO communications with MIMO radar: From co-existence to joint transmission," *IEEE Trans. Wireless Commun.*, vol. 17, no. 4, pp. 2755–2770, Apr. 2018.
- [32] P. Kumari, S. A. Vorobyov, and R. W. Heath, "Adaptive virtual waveform design for millimeter-wave joint communication-radar," *IEEE Trans. Signal Process.*, vol. 68, pp. 715–730, 2020.
- [33] R. Steele and L. Hanzo, "Mobile radio communications: Second and third generation cellular and WATM systems: 2nd." New York, NY, USA: Wiley, 1999.
- [34] A. P. Prudnikov, Y. A. Brychkov, and O. I. Marichev, "*Integrals and series, vol. 1, special functions*," 1986.
- [35] C. Zhang, W. Yi, Y. Liu, and L. Hanzo, "The proofs in the paper titled by 'semi-integrated-sensing-and-communication (Semi-ISaC): From OMA to NOMA'," 2022, arXiv preprint. [Online]. Available: [seetheattachemntsubmittedwiththejournalversion](#).
- [36] Z. Ni, J. A. Zhang, K. Yang, X. Huang, and T. A. Tsiftsis, "Multi-metric waveform optimization for multiple-input single-output joint communication and radar sensing," *IEEE Trans. Commun.*, vol. 70, no. 2, pp. 1276–1289, Feb. 2022.
- [37] C. Li, N. Raymondi, B. Xia, and A. Sabharwal, "Outer bounds for a joint communicating radar (comm-radar): The uplink case," *IEEE Trans. Commun.*, vol. 70, no. 2, pp. 1197–1213, Feb. 2022.

The Proofs in the Paper Titled by “Semi-Integrated-Sensing-and-Communication (Semi-ISaC): From OMA to NOMA”

Chao Zhang, *Graduate Student Member, IEEE*, Wenqiang Yi, *Member, IEEE*,
Yuanwei Liu, *Senior Member, IEEE*, and Lajos Hanzo, *Life Fellow, IEEE*

Abstract

The new concept of semi-integrated-sensing-and-communication (Semi-ISaC) is proposed for next-generation cellular networks. Compared to the conventional ISaC, where the total bandwidth is used for ISaC, the proposed Semi-ISaC framework provides more freedom as it allows that a portion of the bandwidth is exclusively used for wireless communication or radar detection, and the rest is for ISaC transmission. To enhance the bandwidth efficiency (BE), we investigate Semi-ISaC networks both from orthogonal multiple access (OMA) and non-orthogonal multiple access (NOMA), respectively. This paper provides the proof of the journal version submitted to IEEE Transactions of Communications, namely “Semi-Integrated-Sensing-and-Communication (Semi-ISaC): From OMA to NOMA”. This paper provides the proofs of Lemma 1-2, Theorem 1-2, and Corollary 1-2. The other lemmas, theorems, and corollaries have been comprehensively proved in the journal version or similar to the provided proofs.

Index Terms

Semi-integrated-sensing-and-communication, non-orthogonal multiple access, orthogonal multiple access, outage probability, ergodic radar estimation information rate

Chao Zhang, Wenqiang Yi, and Yuanwei Liu are the School of Electronic Engineering and Computer Science, Queen Mary University of London, London E1 4NS, U.K. (email: {chao.zhang, w.yi, yuanwei.liu}@qmul.ac.uk).

L. Hanzo is with the School of Electronics and Computer Science, University of Southampton, Southampton, SO17 1BJ, U.K. (e-mail: lh@ecs.soton.ac.uk).

I. PROOF A: THE PROOF OF LEMMA 1

We formulate the interference of the radar echo as $I_R = P_{BS}\mathcal{P}_r(d_r) \times |h_{r,d}|^2 |h_{r,u}|^2 \gamma^2 B^2 \sigma_\tau^2$. In this expression, we have the small-scale fading parameters as two variables, namely $|h_{r,d}|^2$ and $|h_{r,u}|^2$. We note that both variables obey the Gamma distribution, whose probability density function (PDF) and cumulative distribution function (CDF) are expressed as

$$f_{|h_{r,u}|^2}(x) = f_{|h_{r,d}|^2}(x) = \frac{m^m}{\Gamma(m)} x^{m-1} \exp(-mx), \quad (\text{A.1})$$

$$F_{|h_{r,u}|^2}(x) = F_{|h_{r,d}|^2}(x) = \frac{1}{\Gamma(m)} \gamma(m, mx), \quad (\text{A.2})$$

where $\Gamma(\cdot)$ is the Gamma function and $\gamma(\cdot, \cdot)$ is the lower incomplete Gamma function.

Hence, the expectation of I_R with respect to the variable d_r , namely $\mathbb{E}[I_R](d_r)$, is formulated as

$$\begin{aligned} \mathbb{E}[I_R](d_r) &= P_{BS}\mathcal{P}_r(d_r) \gamma^2 B^2 \sigma_\tau^2 \int_0^\infty x f_{|h_{r,d}|^2}(x) dx \int_0^\infty y f_{|h_{r,u}|^2}(y) dy \\ &= P_{BS}\mathcal{P}_r(d_r) \gamma^2 \beta_{semi}^2 B^2 \sigma_\tau^2 \left(\frac{m^m}{\Gamma(m)} \right)^2 \int_0^\infty x^m \exp(-mx) dx \int_0^\infty y^m \exp(-my) dy, \\ &= P_{BS}\mathcal{P}_r(d_r) \gamma^2 \beta_{semi}^2 B^2 \sigma_\tau^2. \end{aligned} \quad (\text{A.3})$$

Finally, the proof of Lemma 1 is completed.

II. PROOF B: THE PROOF OF THEOREM 1

We have the signal-to-noise ratio (SNR) expression of the OMA user denoted as $\gamma_j^{OMA} = \frac{P_j \mathcal{P}_c(d_j) |h_j|^2}{P_{BS}\mathcal{P}_r(d_r) |h_{r,d}|^2 |h_{r,u}|^2 \gamma^2 B^2 \sigma_\tau^2 + \sigma^2}$. Upon introducing the subscript of $j \in \{c, r\}$ for representing the communication transmitter and the radar target, the expressions of the outage probability (OP) and of the ergodic rate are respectively expressed as

$$\mathbb{P}_j^{OMA} = \Pr \{ \gamma_j^{OMA} < \gamma_{th}^{OMA} \}, \quad (\text{B.1})$$

$$R_j^{OMA} = \frac{1}{2} \log_2 (1 + \gamma_j^{OMA}), \quad (\text{B.2})$$

where γ_{th}^{OMA} is the threshold.

In the following, we will first derive the closed-form OP expression. Upon defining the parameter $\Omega = \frac{m(P_{BS}\mathcal{P}_r(d_r)\gamma^2\beta_{semi}^2B^2\sigma_\tau^2+\sigma^2)}{P_j\mathcal{P}_c(d_j)}$, the OP is formulated as

$$\begin{aligned}
\mathbb{P}_j^{OMA} &= \Pr\{\gamma_j^{OMA} < \gamma_{th}^{OMA}\} \\
&= \Pr\left\{\frac{P_j\mathcal{P}_c(d_j)|h_j|^2}{P_{BS}\mathcal{P}_r(d_r)|h_{r,d}|^2|h_{r,u}|^2\gamma^2B^2\sigma_\tau^2+\sigma^2} < \gamma_{th}^{OMA}\right\} \\
&= \Pr\left\{|h_j|^2 < \frac{(P_{BS}\mathcal{P}_r(d_r)\gamma^2B^2\sigma_\tau^2+\sigma^2)\gamma_{th}^{OMA}}{P_j\mathcal{P}_c(d_j)}\right\} \\
&= \frac{\gamma\left(m, \frac{m(P_{BS}\mathcal{P}_r(d_r)\gamma^2B^2\sigma_\tau^2+\sigma^2)\gamma_{th}^{OMA}}{P_j\mathcal{P}_c(d_j)}\right)}{\Gamma(m)} \\
&= \frac{\gamma(m, \Omega\gamma_{th}^{OMA})}{\Gamma(m)}. \tag{B.3}
\end{aligned}$$

We then derive the closed-form expression of the ergodic rate, yielding the following expression:

$$\begin{aligned}
R_j^{OMA} &= \frac{1}{2}\log_2(1 + \gamma_j^{OMA}) \\
&= \frac{1}{2\ln 2} \int_0^\infty \frac{1 - \mathbb{P}_j^{OMA}(\gamma_{th}^{OMA})}{1+x} dx \\
&\stackrel{(a)}{=} \frac{1}{2\ln 2} \sum_{k=0}^{m-1} \frac{\Omega^k}{k!} \int_0^\infty \frac{x^k \exp(-\Omega x)}{1+x} dx \\
&\stackrel{(b)}{=} \frac{1}{2\ln 2} \sum_{k=0}^{m-1} \frac{\Omega^k}{k!} \exp(\Omega) \Gamma(k+1) \Gamma(-k, \Omega), \tag{B.4}
\end{aligned}$$

where we derive the step (a) by exploiting the series expansion of the incomplete Gamma function denoted as $\gamma(m, t) = (m-1)! - \exp(-t) \sum_{k=0}^{m-1} \frac{(m-1)!}{k!} t^k$. We then derive the step (b) by exploiting the integral denoted as $\int_0^\infty \frac{x^a}{1+x} \exp(-bx) = \exp(b) \Gamma(a+1) \Gamma(-a, b)$.

Finally, based on the relationship between the generalized exponential integral (namely $E_n(\cdot)$) and the upper incomplete Gamma function with negative parameters (denoted as $\Gamma(-k, \Omega) = \frac{E_{1+k}(\Omega)}{\Omega^k}$), we formulate the final expression of the ergodic rate:

$$R_j^{OMA} = \frac{1}{2\ln 2} \sum_{k=0}^{m-1} \exp(\Omega) E_{1+k}(\Omega). \tag{B.5}$$

Hence, the proof of the Theorem 1 is completed.

III. PROOF C: THE PROOF OF LEMMA 2

Since we have both $|h_{r,d}|^2$ and $|h_{r,u}|^2$ obeying the Gamma distribution, the PDF and CDF of the multiplication of both variables, namely $f_{|h_{r,d}|^2|h_{r,u}|^2}(x)$ and $F_{|h_{r,d}|^2|h_{r,u}|^2}(x)$, are expressed as

$$\begin{aligned} f_{|h_{r,d}|^2|h_{r,u}|^2}(z) &= \int_0^\infty \frac{1}{x} f_{|h_{r,d}|^2}(x) f_{|h_{r,u}|^2}\left(\frac{z}{x}\right) dx \\ &\stackrel{(a)}{=} \frac{m^{2m} z^{m-1}}{(\Gamma(m))^2} \int_0^\infty \frac{1}{x} \exp\left(-m\left(x + \frac{z}{x}\right)\right) dx \\ &\stackrel{(b)}{=} \frac{2m^{2m}}{(\Gamma(m))^2} z^{m-1} K_0(2m\sqrt{z}), \end{aligned} \quad (\text{C.1})$$

where $K_0(\cdot)$ is the modified Bessel function of the third kind. The step (a) is obtained by substituting the PDF of the Gamma distribution (Eq. (A.1)). The step (b) is formulated by exploiting Eq.[2.3.6.7] of [34] in the journal version.

Since we have the transformation between the modified Bessel function and the Meijer-G function expressed as $K_v(x) = \frac{1}{2} G_{02}^{20}\left(\frac{x^2}{4} \left| \begin{smallmatrix} \cdot \\ \frac{v}{2}, -\frac{v}{2} \end{smallmatrix} \right.\right)$, where $G_{p\ q}^{mn}\left(\cdot \left| \begin{smallmatrix} (a_p) \\ (b_q) \end{smallmatrix} \right.\right)$ is the Meijer-G function, we further formulate the PDF expression as

$$f_{|h_{r,d}|^2|h_{r,u}|^2}(z) = \frac{m^{2m}}{(\Gamma(m))^2} z^{m-1} G_{02}^{20}(m^2 z \left| \begin{smallmatrix} \cdot \\ \cdot \end{smallmatrix} \right.). \quad (\text{C.2})$$

Based on the PDF expressed as Eq. (C.2), we then derive the CDF of $f_{|h_{r,d}|^2|h_{r,u}|^2}(x)$ as

$$\begin{aligned} F_{|h_{r,d}|^2|h_{r,u}|^2}(x) &= \frac{2m^{2m}}{(\Gamma(m))^2} \int_0^x z^{m-1} K_0(2m\sqrt{z}) dz \\ &\stackrel{(a)}{=} \frac{m^{2m}}{(\Gamma(m))^2} \int_0^x z^{m-1} G_{02}^{20}(m^2 z \left| \begin{smallmatrix} \cdot \\ \cdot \end{smallmatrix} \right.) dz \\ &\stackrel{(b)}{=} \frac{m^{2m}}{(\Gamma(m))^2} x^m G_{13}^{21}(m^2 x \left| \begin{smallmatrix} 1-m \\ 0, 0, -m \end{smallmatrix} \right.) \\ &\stackrel{(c)}{=} \frac{G_{13}^{21}(m^2 x \left| \begin{smallmatrix} 1 \\ m, m, 0 \end{smallmatrix} \right.)}{(\Gamma(m))^2}, \end{aligned} \quad (\text{C.3})$$

where the step (a) is derived by exploiting $K_v(x) = \frac{1}{2} G_{02}^{20}\left(\frac{x^2}{4} \left| \begin{smallmatrix} \cdot \\ \frac{v}{2}, -\frac{v}{2} \end{smallmatrix} \right.\right)$. The step (b) is derived by exploiting the integral of $\int_0^y x^{\alpha-1} G_{p\ q}^{mn}\left(wx \left| \begin{smallmatrix} (a_p) \\ (b_q) \end{smallmatrix} \right.\right) dx = y^\alpha G_{p+1\ q+1}^{m\ n+1}\left(wy \left| \begin{smallmatrix} a_1, \dots, a_n, \dots, 1-\alpha; a_n, \dots, a_p \\ b_1, \dots, b_m, \dots, -\alpha, b_{m+1}, \dots, b_q \end{smallmatrix} \right.\right)$. Additionally, the step (c) is formulated by using $z^p G_{p\ q}^{mn}\left(z \left| \begin{smallmatrix} (a_p) \\ (b_q) \end{smallmatrix} \right.\right) = z^p G_{p\ q}^{mn}\left(z \left| \begin{smallmatrix} (a_p)+p \\ (b_q)+p \end{smallmatrix} \right.\right)$.

Finally, we complete the proof of Lemma 2 by the final expressions, namely Eq. (C.1) and Eq. (C.3).

IV. PROOF D: THE PROOF OF THEOREM 2 AND COROLLARY 1

We provide the proofs of Theorem 2 and Corollary 1 jointly in this section. For the analytical results of the radar echoes, the expression of the ergodic REIR is formulated directly by exploiting Eq. (C.3), yielding

$$\begin{aligned}
 R_{est} &\leq \frac{\delta}{2T} \log_2 \left(1 + \Xi_{r,1}(d_r)^{-\alpha_r} |h_{r,d}|^2 |h_{r,u}|^2 \right) \\
 &= \frac{\delta}{2T \ln(2)} \int_0^\infty \frac{1}{z+1} \left(1 - F_{|h_{r,d}|^2 |h_{r,u}|^2} \left(\frac{d_t^{\alpha_r}}{\Xi_{r,1}} z \right) \right) dz \\
 &= \frac{\delta}{2T \ln(2)} \int_0^\infty \frac{1}{z+1} \left(1 - \frac{G_{13}^{21} \left(\frac{m^2 d_t^{\alpha_r}}{\Xi_{r,1}} z \mid_{m,m,0}^1 \right)}{(\Gamma(m))^2} \right) dz, \tag{D.1}
 \end{aligned}$$

where we have $\Xi_{r,1} = \frac{2TP_{BS}\gamma^2 B^2 \sigma_z^2 G_r C_r (d_r)^{-\alpha_r}}{k_B T_{temp}}$.

Upon considering $m = 1$ as a special case, we further derive the above equation Eq. (D.1) as

$$\begin{aligned}
 R_{est} &\leq \frac{\delta}{2T} \log_2 \left(1 + \Xi_{r,1}(d_r)^{-\alpha_r} |h_{r,d}|^2 |h_{r,u}|^2 \right) \\
 &\stackrel{(a)}{=} \frac{\delta}{2T \ln(2)} \int_0^\infty \int_0^\infty \frac{1}{z+1} \left(1 - F_{|h_{r,d}|^2} \left(\frac{d_t^{\alpha_r}}{\Xi_{r,1}x} z \right) \right) f_{|h_{r,u}|^2}(x) dx dz \\
 &\stackrel{(b)}{=} \frac{\delta}{2T \ln(2)} \int_0^\infty \int_0^\infty \frac{\exp\left(-\frac{d_t^{\alpha_r} z}{\Xi_{r,1}x}\right)}{z+1} dz \exp(-x) dx \\
 &\stackrel{(c)}{=} \frac{-\delta}{2T \ln(2)} \int_0^\infty \exp\left(\frac{d_t^{\alpha_r}}{\Xi_{r,1}x}\right) \text{Ei}\left(-\frac{d_t^{\alpha_r}}{\Xi_{r,1}x}\right) \exp(-x) dx \\
 &\stackrel{(d)}{=} \frac{-\delta}{2T \ln(2)} \int_0^\infty x^{-2} \exp\left(\frac{d_t^{\alpha_r} x}{\Xi_{r,1}} - \frac{1}{x}\right) \text{Ei}\left(-\frac{d_t^{\alpha_r}}{\Xi_{r,1}x}\right) dx \\
 &\stackrel{(e)}{=} \frac{\delta}{2T \ln(2)} G_{13}^{31} \left(d_t^{\alpha_r} \Xi_{r,1}^{-1} \mid_{0,0,1}^0 \right), \tag{D.2}
 \end{aligned}$$

where $\text{Ei}(\cdot)$ is the exponential integral. We express the probability of both variables by integrals, yielding the step (a). Additionally, we substitute the PDF of the Gamma distribution (Eq. (A.1)) into the step (a) of Eq. (D.2), yielding the step (b). Then, we exploit the Eq.[2.3.4.4] of [34] to obtain the step (c). We further derive the step (d) by replacing $\frac{1}{x}$ by x . Finally, we have the step (e) by using the integral of $\int_0^\infty x^{-2} \exp\left(Ax - \frac{1}{x}\right) \text{Ei}(-Ax) dx = G_{13}^{31} \left(A \mid_{0,0,1}^0 \right)$. And the proofs of Theorem 2 and Corollary 1 are completed.

V. PROOF E: THE PROOF OF COROLLARY 2

Based on Theorem 3, we have the outage probability expression of the communication transmitter as

$$\begin{aligned} \mathbb{P}_c^I = & 1 - \exp\left(-\frac{m\gamma_{th}}{P_c}(a_1 + a_2)\right) \sum_{p=0}^{m-1} \frac{m^r \gamma_{th}^p}{(m-1)!p!} \\ & \times \sum_{r=0}^p C_p^r \frac{(a_1 + a_2)^r (P_r a_3)^{p-r}}{P_c^p} \Gamma(m+p-r) \left(\frac{\gamma_{th} a_3 P_r}{P_c} + 1\right)^{-(m+p-r)}, \end{aligned} \quad (\text{E.1})$$

where we have $a_1 = \frac{P_{BS} G_r C_r (d_r)^{-\alpha_r} \gamma^2 \beta_{sem}^2 B^2 \sigma_\tau^2}{G_c C_c (d_c)^{-\alpha_c}}$, $a_2 = \frac{\sigma^2}{G_c C_c (d_c)^{-\alpha_c}}$, $a_3 = \frac{(d_r)^{-\alpha_c}}{(d_c)^{-\alpha_c}}$, and $C_n^m = n!/(m!(n-m)!)$.

In Scenario-I, the ergodic rate of the communication transmitter in the NOMA-based Semi-ISAC scenario is formulated as

$$R_c^{er,I} = \frac{1}{\ln 2} \int_0^\infty \frac{1 - \mathbb{P}_c^I(\gamma_{th})}{1 + \gamma_{th}} d\gamma_{th}. \quad (\text{E.2})$$

We substitute Eq. (E.1) into Eq. (E.3), yielding the further expression of the ergodic rate

$$\begin{aligned} R_c^{er,I} = & \frac{1}{\ln 2} \sum_{p=0}^{m-1} \frac{m^r}{(m-1)!p!} \sum_{r=0}^p C_p^r \frac{(a_1 + a_2)^r (P_r a_3)^{p-r}}{P_c^p} \Gamma(m+p-r) \\ & \times \int_0^\infty \frac{x^p}{1+x} \left(\frac{x a_3 P_r}{P_c} + 1\right)^{-(m+p-r)} \exp\left(-\frac{mx}{P_c}(a_1 + a_2)\right) dx \\ \stackrel{(a)}{=} & \frac{1}{\ln 2} \sum_{p=0}^{m-1} \frac{m^r}{(m-1)!p!} \sum_{r=0}^p C_p^r \frac{(a_1 + a_2)^r (P_r a_3)^{p-r}}{P_c^p} \Gamma(m+p-r) \\ & \times \sum_{k=0}^\infty \binom{m+p-r+k-1}{k} \left(-\frac{a_3 P_r}{P_c}\right)^k \int_0^\infty \frac{x^{p+k}}{1+x} \exp\left(-\frac{m(a_1 + a_2)}{P_c}x\right) dx \\ \stackrel{(b)}{=} & \frac{1}{\ln 2} \sum_{p=0}^{m-1} \sum_{r=0}^p C_p^r \frac{\Lambda_1^{r-(1+p+k)} (P_r a_3)^{p-r}}{(m-1)!p! P_c^{p-r}} \Gamma(m+p-r) \\ & \times \sum_{k=0}^\infty \binom{m+p-r+k-1}{k} \left(-\frac{a_3 P_r}{P_c}\right)^k \exp(\Lambda_1) \Gamma(p+k+1) E_{1+p+k}(\Lambda_1), \end{aligned} \quad (\text{E.3})$$

where we have $\Lambda_1 = \frac{m(a_1+a_2)}{P_c}$. The step (a) is formulated by exploiting the binomial expansion with negative exponents, denoted as $(1+x)^{-n} = \sum_{k=0}^\infty \binom{n+k-1}{k} (-x)^k$. Since we have the expression of $E_n(x) = x^n \Gamma(1-n, x)$, the step (b) is formulated by exploiting the following

derivation:

$$\begin{aligned}
& \int_0^\infty \frac{x^{p+k}}{1+x} \exp\left(-\frac{m(a_1+a_2)}{P_c}x\right) dx \\
&= \exp\left(\frac{m(a_1+a_2)}{P_c}\right) \Gamma(p+k+1) \Gamma\left(-p-k, \frac{m(a_1+a_2)}{P_c}\right) \\
&= \exp\left(\frac{m(a_1+a_2)}{P_c}\right) \Gamma(p+k+1) \left(\frac{m(a_1+a_2)}{P_c}\right)^{-(1+p+k)} E_{1+p+k}\left(\frac{m(a_1+a_2)}{P_c}\right). \quad (\text{E.4})
\end{aligned}$$

Hence, the proof of Corollary 2 is completed.